Thermodynamics and Reaction Mechanisms for Decomposition of a Simple Protonated Tripeptide, H<sup>+</sup>GGA: From H<sup>+</sup>GGG to H<sup>+</sup>GAG to H<sup>+</sup>GGA

Abhigya Mookherjee and P. B. Armentrout\*

Department of Chemistry, University of Utah, 315 S.1400 E. Rm 2020, Salt Lake City, UT 84112, United States

Abstract: We present a thorough characterization of fragmentations observed in threshold collision-induced dissociation (TCID) experiments of protonated glycylglycylalanine (H<sup>+</sup>GGA) with Xe using a guided ion beam tandem mass spectrometer. Kinetic energy dependent cross sections for nine ionic products were obtained and analyzed to provide 0 K barriers for the five primary products:  $[b_2]^+$ ,  $[y_1 + 2H]^+$ ,  $[b_3]^+$ ,  $[y_2 + 2H]^+$ , and  $[a_1]^+$ ; and four secondary products:  $[a_2]^+$ , [a<sub>3</sub>]<sup>+</sup>, high-energy [y<sub>1</sub> + 2H]<sup>+</sup>, and CH<sub>3</sub>CHNH<sub>2</sub><sup>+</sup>, after accounting for multiple ion-molecule collisions, internal energy of reactant ions, unimolecular decay rates, competition between channels, and sequential dissociations. Relaxed potential energy surface scans performed at the B3LYP-GD3BJ/6-311+G(d,p) level of theory are used to identify transition states (TSs) and intermediates of the five primary and three secondary products (with the mechanism of the other secondary product previously established). Geometry optimizations and single point energy calculations of reactants, products, intermediates, and TSs were performed at several levels of theory. These theoretical energies are compared with experimental threshold energies and found to give reasonable agreement, with B3LYP-GD3BJ and M06-2X levels of theory performing slightly better than MP2 and better than B3LYP. The results obtained here are compared with previous results for decomposition of H<sup>+</sup>GGG and H<sup>+</sup>GAG to probe the effect of changing amino acid sequence. Methylation in H<sup>+</sup>GGA has a significant effect on the competition between the primary sequence products,  $[b_2]^+$  and  $[y_1 + 2H]^+$ , suppressing the  $[b_2]^+$  cross section by raising its threshold energy, while enhancing that of  $[y_1 + 2H]^+$  by lowering its threshold energy.

\*Correspondence to P. B. Armentrout, email: armentrout@chem.utah.edu; ORCID: 0000-0003-

#### Introduction

Knowledge of the amino acid sequence of a peptide/protein is essential for its unambiguous identification. Tandem mass spectrometry (MS/MS) remains the routinely used analytical tool of choice for determining this primary structure, which is often attained by collision-induced dissociation (CID). At low collision energies, CID of protonated peptides forms sequence ions,  $[b_n]^+$  and  $[y_n + 2H]^+$ , that are formed by amide bond cleavage. These primary products can further dissociate to yield  $[b_m]^+$ ,  $[y_m + 2H]^+$ ,  $[a_n]^+$  ions, internal fragments, and immonium ions at higher collision energies. (Here, the nomenclature used for peptide fragment ions is adopted from the "all-explicit" nomenclature proposed by Chu et al., a modification of that proposed by Roepstorff and Fohlmann, and Biemann. Often fragment ions are also formed by the loss of neutrals like water, carbon monoxide, or ammonia. Along with structural information, CID studies of peptides can also provide information on the reaction mechanisms by which the fragmentations occur.

In the present work, absolute cross sections for decomposition of protonated glycylglycylalanine (H<sup>+</sup>GGA) were measured with a sensitivity of over three orders of magnitude over a center-of-mass collision energy range of 0 – 9 eV. The experimental results were analyzed using molecular parameters (vibrational frequencies and rotational constants) determined in theoretical calculations to extract absolute experimental threshold energies for all primary and several secondary fragmentation pathways. The experimental threshold energies are compared with those obtained from single point energy calculations performed at the B3LYP,<sup>4-5</sup> B3LYP-D3 (B3LYP with the GD3BJ dispersion correction),<sup>6-7</sup> MP2(full),<sup>8</sup> and M06-2X<sup>9</sup> levels of theory. This allows us to compare the measured threshold energies with computed threshold energies, in turn allowing the identification of the key steps involved in H<sup>+</sup>GGA fragmentation as well as the structures of the products. Comparison of these results to those of protonated glycylglycylglycine (H<sup>+</sup>GGG) <sup>10</sup> and glycylalanylglycine (H<sup>+</sup>GAG) <sup>11</sup> permit understanding and quantification of the effects of methylation on the threshold energies of primary sequence ions. Indeed, this work is part

of a systematic study that we have undertaken to understand the effects of methylation – specifically tracking and quantifying the fragmentation propensities and reaction mechanisms when the amino acid sequence is minutely changed from protonated GGG to GAG and then to GGA.

#### **Experimental and Computational Details**

### Experimental Procedures

Cross-sections of H<sup>+</sup>GGA colliding with Xe were measured using a guided ion beam tandem mass spectrometer (GIBMS) that has been described in detail previously. <sup>12-13</sup> The H<sup>+</sup>GGA ions were generated using an electrospray ionization source (ESI) <sup>14</sup> under conditions similar to those described earlier, such that the H<sup>+</sup>GGA ions were characterized by a temperature of 300 K <sup>14-18</sup>. Details of the experimental methods and means of data analysis <sup>19-21</sup> can be found in the Supporting Information. In the data analysis, when reactions are limited by loose transition states (TSs), TS frequencies equal those of the dissociated products with transitional frequencies treated as rotors in the phase space limit (PSL). <sup>20-21</sup> For reactions limited by tight TSs, molecular parameters were taken directly from theoretical results for the rate-limiting TS structures, described below. All energies reported below are in the center-of-mass (CM) frame unless otherwise noted.

### Data Analysis

Details of the modeling of the data to extract thermodynamic information are provided in the Supporting Information. In all cases discussed below, vibrational frequencies for the TS of each reaction channel were taken from the theoretical results discussed in the next section. As will be seen, low-frequency modes (<900 cm<sup>-1</sup>) of some TSs need to be modified slightly in order to accurately reproduce the relative shapes (energy dependences) and magnitudes of the competing product cross sections. In the study where we originally used this approach,<sup>22</sup> we noted that similar results can be obtained by scaling the magnitudes of the cross section models, but this often

required physically unmeaningful scaling factors approaching  $10^3 - 10^6$ . In contrast, the Gaussian program points out that calculations of vibrational frequencies below about 900 cm<sup>-1</sup> are subject to considerable uncertainty because they may no longer be treated accurately as harmonic. Details are discussed in the Supporting Information.

#### Computational Procedures

The Gaussian 09 suite of programs<sup>23</sup> was used to calculate geometries, vibrational frequencies, and energies of reactants, products, intermediates, and TSs. Key TSs, intermediates, and products were initially guessed on the basis of the analogous species found in the H<sup>+</sup>GGG and H<sup>+</sup>GAG computational studies. <sup>10-11</sup> Optimizations of all low-lying structures were performed at the B3LYP/6-311+G(d,p) level of theory. We also performed relaxed potential energy surface (PES) scans at B3LYP/6-31+G(d) or B3LYP/6-311+G(d,p) levels of theory to identify elementary steps in the transformations and decompositions of H<sup>+</sup>GGA and its products (details below). TSs and intermediates occurring along the PESs were then optimized at the B3LYP/6-311+G(d,p) level, where each TS was verified to contain one imaginary frequency and each intermediate is vibrationally stable. Rate-limiting TSs were further examined with an intrinsic reaction coordinate (IRC) calculation to verify that they connect the appropriate intermediates. Rotational constants and vibrational frequencies were also calculated at the B3LYP/6-311+G(d,p) level of theory. Vibrational frequencies were scaled by 0.989 24 before being used in the modeling process to calculate zero-point energy (ZPE) and thermal corrections. Using these geometries and ZPE corrections, single point energies (SPEs) were computed at both B3LYP and MP2(full) (where full refers to correlation of all electrons) levels of theory using the 6-311+G(2d,2p) basis set. We also performed geometry optimizations of key reactant conformers, TSs, and products at the B3LYP/6-311+G(d,p) level of theory using an empirical dispersion correction, GD3BJ (abbreviated as B3LYP-D3 in this study) and at the M06-2X/6-311+G(d,p) level of theory. For these species, SPEs were then calculated at the B3LYP-D3 and M06-2X levels of theory, respectively, using a slightly bigger 6-311+G(2d,2p) basis set. For simplicity, the B3LYP/B3LYP, B3LYP-D3/B3LYP-D3, M06-2X/M06-2X, and MP2(full)//B3LYP SPEs will be referred to as B3LYP, B3LYP-D3, M06-2X, and MP2 in the remaining text.

### Nomenclature

Conformers of H<sup>+</sup>GGA are named using the same nomenclature used in the H<sup>+</sup>GGG and H<sup>+</sup>GAG studies  $^{10\text{-}11}$  where the site of protonation is designated within square brackets, followed by designation of eight dihedral angles starting from the N terminus and going along the backbone of H<sup>+</sup>GGA to the hydroxy group: c (cis for angles between  $0^{\circ}$  -  $45^{\circ}$ ), g (gauche for  $45^{\circ}$  -  $135^{\circ}$ ), and t (trans for  $135^{\circ}$  -  $180^{\circ}$ ). Atoms are numbered according to their residue with a superscript. Product conformers are named in a similar manner defining the protonation site and the relevant dihedral angles. Transition states are indicated by TS followed by a description of the change in the protonation site, dihedral angle, or bond cleavage. For example, the TS for a proton transfer is named TS[O<sup>1</sup>-N<sup>1</sup>] indicating transfer of a proton from the carbonyl oxygen O<sup>1</sup> (the lower energy conformer is listed first) to the amide nitrogen N<sup>1</sup>. A TS involving a dihedral angle change is designated within parentheses, e.g., (cg) which indicates that the dihedral angle changes from cis (the lower energy conformer) to gauche. A TS involving bond cleavage indicates the bond being broken by  $\sim$  inside curly brackets, e.g.,  $\{OC\sim N^2\}$ .

#### **Results**

Cross Sections for Collision-Induced Dissociation

Figure 1 shows the experimental kinetic energy dependent cross sections obtained for the interaction of H<sup>+</sup>GGA with Xe. Nine ionic products are observed for H<sup>+</sup>GGA (m/z 204) fragmentation. On the basis of the theoretical results, these are assigned to reactions 1 - 8. The sequence of these reactions is outlined in Scheme 1 which also includes the unobserved intermediate (CH<sub>2</sub>NH)H<sup>+</sup>(GA) (m/z 176).

$$H^+GGA + Xe \rightarrow C_4H_7N_2O_2^+([b_2]^+, H^+AMOx) + C_3H_7NO_2(A) + Xe$$
 (1)

$$\rightarrow C_3H_8NO_2^+([y_1 + 2H]^+, H^+A) + C_4H_6N_2O_2(AMO_X) + Xe$$
 (2a)

$$\rightarrow C_3H_8NO_2^+([y_1+2H]^+, H^+A) + 2CO + 2CH_2NH + Xe$$
 (2b)

$$\rightarrow C_7 H_{12} N_3 O_3^+ ([b_3]^+, H^+ GAMMOx) + H_2 O + Xe$$
 (3)

$$\rightarrow C_5H_{11}N_2O_3^+([y_2+2H]^+, H^+GA) + CO + CH_2NH + Xe$$
 (4)

$$\rightarrow \text{CH}_2\text{NH}_2^+([a_1]^+) + \text{CO} + \text{C}_5\text{H}_{10}\text{N}_2\text{O}_3 \text{ (GA)} + \text{Xe}$$
 (5a)

$$\rightarrow \text{CH}_2\text{NH}_2^+([a_1]^+) + 2\text{CO} + \text{CH}_2\text{NH} + \text{C}_3\text{H}_7\text{NO}_2(A) + \text{Xe}$$
 (5b)

$$\rightarrow C_3H_7N_2O^+([a_2]^+) + CO + C_3H_7NO_2(A) + Xe$$
 (6)

$$\rightarrow$$
 CH<sub>3</sub>CHNH<sub>2</sub><sup>+</sup> (44, [y<sub>1</sub> + 2H - CO - H<sub>2</sub>O]<sup>+</sup>) + CO + H<sub>2</sub>O + AMOx + Xe (7)

$$\rightarrow C_6 H_{12} N_3 O_2^+ ([a_3]^+) + H_2 O + C O + X e$$
 (8)

Figure 1 shows that the total cross section increases smoothly with increasing energy consistent with the coupled and sequential nature of reactions 1-8. The dominant low-energy product arises from the loss of alanine to form the  $[b_2]^+$  ion (m/z 115) in reaction 1. As identified originally by Harrison and co-workers<sup>25</sup> and later by many other studies, <sup>26-34</sup> [b<sub>2</sub>]<sup>+</sup> is protonated 2-aminomethyl-5-oxazolone (H<sup>+</sup>AMOx). Arising at about the same energy and magnitude is the  $[y_1 + 2H]^+$  (m/z90, protonated alanine) ion in reaction 2a, which directly competes with [b<sub>2</sub>]<sup>+</sup> because reactions 1 and 2a differ only in which fragment keeps the proton. After rising to about 4 Å<sup>2</sup> and declining to ~2 Å<sup>2</sup>, this cross section rises again beginning near 5 eV, indicating the contribution of a new pathway to this product, reaction 2b. This high-energy (HE) portion of the  $[y_1 + 2H]^+$  cross section will be henceforth referred to as  $[y_1 + 2H]^+_{HE}$ . The next largest low-energy cross section is associated with the formation of  $[y_2 + 2H]^+$  (m/z 147), which is protonated glycylalanine (GA), formed in reaction 4. This  $[y_2 + 2H]^+$  product dissociates to form  $[y_1 + 2H]^+_{HE}$  in reaction 2b, consistent with a drop in the  $[y_2 + 2H]^+$  cross section at  $\sim 5.5$  eV that is concomitant with the increase in the  $[y_1 + 2H]^+$  cross section at high energies. Formation of  $[b_3]^+$  (m/z 186) in reaction 3 starts at about the same apparent threshold as  $[b_2]^+$  and  $[y_1 + 2H]^+$  and corresponds to the formation of protonated 2-glycylaminomethyl-(4-methyl-5-oxazolone) (H<sup>+</sup>GAMMOx) by loss of water from H<sup>+</sup>GGA. The next product observed in Figure 1 is formed in reaction 8 by the loss of CO from  $[b_3]^+$  to yield  $[a_3]^+$  (m/z 158). Next comes generation of  $[a_2]^+$  (m/z 87) in reaction 6 by the loss of CO from [b<sub>2</sub>]<sup>+</sup>, where the cross section shown has been corrected for mass overlap from

m/z 90. The decline of  $[b_2]^+$  is consistent with the rise of  $[a_2]^+$  at about 4 eV, Figure 1. At about the same apparent threshold as  $[a_2]^+$ ,  $CH_3CHNH_2^+$  (m/z 44) can be formed in reaction 7 by loss of CO +  $H_2O$  from the low-energy  $[y_1 + 2H]^+$  product, which is consistent with the decline in the  $[y_1 + 2H]^+$  cross-section at ~ 2.6 eV. The dissociation of  $[y_1 + 2H]^+$  by loss of CO +  $H_2O$  has been observed in previous works.<sup>11,35</sup>

The product having the highest apparent threshold energy is the [a<sub>1</sub>]<sup>+</sup> (*m/z* 30) product formed in reactions 5. This product has a cross section that is the largest of all products at high energies, which can be attributed to the multiple pathways that are capable of yielding [a<sub>1</sub>]<sup>+</sup>. The lowest energy pathway is reaction 5a, which competes directly with reaction 4. Reaction 5b can occur either by dissociation of [a<sub>2</sub>]<sup>+</sup> or [y<sub>2</sub> + 2H]<sup>+</sup>, as observed in previous studies.<sup>10, 32, 36-37</sup> Although both reactions 4 and 5a are initiated by loss of CO, no primary ion at the appropriate mass (*m/z* 176) was observed, despite carefully looking for it. This can occur if CO loss involves a tight transition state (TTS) such that loss of additional fragments from *m/z* 176 occurs readily at the energy of the TTS. This is consistent with our previous observations in studies of H<sup>+</sup>GGG and H<sup>+</sup>GAG <sup>10-11</sup> and the low-energy milli-second ion trap/ CID studies of H<sup>+</sup>AGG by Bythell et al.<sup>38</sup> Notably, these authors did observe the analogous product ion for loss of CO in MALDI/TOF/TOF, sector metastable ion (MI), and sector CID experiments that occur at faster (microsecond) timescales and higher energies. Finally, in our previous studies of H<sup>+</sup>GGG and H<sup>+</sup>GAG, we observed a product corresponding to the combined losses of CO + NH<sub>3</sub>, which competes with the analogous of reactions 4 and 5a. The analogous process was not observed in the present system.

### H<sup>+</sup>GGA Ground Structure

Figure 2 shows the six lowest energy conformations of H<sup>+</sup>GGA located in the present study and their relative energies (also listed in Supporting Table S1). Two of the structures,  $[O^{1t}]$ -ctgttttt and  $[O^{1t}]$ -ctgttgtt, involve protonation at the carbonyl oxygen of the first residue  $(O^{1})$  with the proton directed towards  $O^{2}$  (as indicated by the superscript t denoting the trans orientation of the  $\angle CCO^{1}H$  dihedral angle). B3LYP, B3LYP-D3, and M06-2X calculations suggest the  $[O^{1t}]$ -ctgttttt

conformer is the global minimum (GM) and all levels of theory place the  $[O^{1t}]$ -ctgttgtt structure 5 – 7 kJ/mol higher. Both  $[O^{1t}]$ -ctgttttt and  $[O^{1t}]$ -ctgttgtt are stabilized by  $N^2H \cdot N^1$ ,  $O^1H \cdot O^2$ , and  $O^4H \cdot O^3$  hydrogen bonds, with the former being stabilized by an additional  $N^3H \cdot O^3$  hydrogen bond. Both structures have trans peptide bonds ( $\angle$ CCNC) as reflected by the second and fifth dihedral angle designation in our nomenclature. Four of the structures shown in Figure 2 are protonated at their ( $N^1$ ) nitrogen, with  $[N^1]$ -ttggtgtt being the only one having a trans peptide bond between the first and second residue (as indicated by the second dihedral angle designation). At the MP2 level of theory, three of these structures,  $[N^1]$ -tcgctgtt,  $[N^1]$ -ttggtgtt, and  $[N^1]$ -gcgttgtt lie below  $[O^{1t}]$ -ctgttttt by 2-5 kJ/mol, where  $[N^1]$ -tcgctgtt is the GM with the latter two structures higher by only 1-2 kJ/mol. The DFT levels of theory place these four  $[N^1]$  structures 7-20 (ttggtgtt), 4-26 (gcgttgtt), 4-18 (tcgctgtt), and 13-20 (gcgttttt) kJ/mol above their  $[O^{1t}]$ -ctgttttt GM.

Conformers directly analogous to those shown in Figure 2 were also found for the H<sup>+</sup>GGG and H<sup>+</sup>GAG conformers, <sup>10-11</sup> which is reasonable because the methyl side chains do not participate in the hydrogen bonding that determines their structures. These conformers have similar relative energies and the same names because the side-chains are not involved in the nomenclature.

In our H<sup>+</sup>GGG study,  $^{10}$  we compared the infrared spectra calculated for  $[O^{1\tau}]$ -ctgttttt,  $[N^1]$ -gcgttgtt,  $[N^1]$ -ttggtgtt, and  $[N^1]$ -tcgctgtt conformers with the infrared multiple photon dissociation (IRMPD) spectrum obtained by Wu and McMahon.  $^{39}$  This comparison suggested that both  $[O^{1\tau}]$ -ctgttttt and  $[N^1]$ -ttggtgtt were present for H<sup>+</sup>GGG formed under ESI conditions, whereas no evidence was found for the cis peptide bonded conformers. These results were rationalized on the basis of calculations that indicated that the trans-cis peptide bond isomerization required 58-71 kJ/mol, such that trans-cis isomerization would not occur under ESI conditions or in solution. Because most peptides are known to adopt trans peptide bonds in solution, these results suggested that only the trans peptide conformers are accessible in the ESI source. Similar trans-cis isomerization of the peptide bond in H<sup>+</sup>GAG  $[N^1]$ -gcgttgtt was found to require 67-87 kJ/mol.  $^{11}$  In the present system, the TS for trans-cis isomerization of the first peptide bond in H<sup>+</sup>GGA is  $TS([N^1]$ -g(ct)gttttt), Figure 3, and lies 64-82 kJ/mol above the GM, Table S3. As all these

isomerization TS energies are comparable, this comparison suggests that H<sup>+</sup>GGA conformers containing only trans peptide bonds are formed in the ESI source.

This conclusion is clouded by an IR-IR double resonance cryogenic ion vibrational predissociation spectroscopic (CIVS) investigation of H<sup>+</sup>GGG,<sup>40</sup> which found [O<sup>1t</sup>]-ctgttttt and [N<sup>1</sup>]-gcgttgtt as the dominant conformers of H<sup>+</sup>GGG. Notably, in the CIVS investigation, the H<sup>+</sup>GGG ions made in the ESI at 300 K were collisionally cooled to 10 K such that kinetic trapping of conformers is possible. Nevertheless, this study indicates that an ESI source can form conformers with a cis peptide bond.

It can be realized that the isomerization barrier is well below the energies needed for decomposition, such that it does not matter whether a conformer having a trans or cis peptide bond is generated in the ESI source because they can readily interconvert at the energies needed for fragmentation. Indeed, we have recently demonstrated that such interconversion occurs readily in the H<sup>+</sup>GPA (protonated glycylprolinylalanyl) tripeptide<sup>41</sup> and previous studies drew similar conclusions for systems having functionalized side-chains (arginine<sup>42</sup> and histidine<sup>43</sup>). Thus, on the basis of similarities with our previous examinations of H<sup>+</sup>GGG and H<sup>+</sup>GAG, and the energetics of trans-cis isomerization, we assign the [N<sup>1</sup>]-ttggtgtt conformer as the MP2 GM. As a result, Figure 2 and Supporting Tables S1-S3 list DFT energies of all species relative to [O<sup>1t</sup>]-ctgttttt and MP2 energies relative to [N<sup>1</sup>]-ttggtgtt. Because MP2 finds that the [N<sup>1</sup>]-tcgctgtt species lies only 1.1 kJ/mol below [N<sup>1</sup>]-ttggtgtt, irrespective of whether the species formed experimentally is [N<sup>1</sup>]-ttggtgtt or [N<sup>1</sup>]-tcgctgtt, the comparison of theoretical and experimental energies is not compromised.

### $[b_2]^+/[y_1 + 2H]^+$ Formation

The reaction mechanism for the formation of  $[b_2]^+$  and  $[y_1 + 2H]^+$  ions from peptides similar to H<sup>+</sup>GGA has been studied previously. <sup>10-11, 26-27, 38, 44</sup> Unsurprisingly, the reaction mechanisms for H<sup>+</sup>GGA decompositions are directly analogous to those found for H<sup>+</sup>GGG and H<sup>+</sup>GAG decompositions, which have been described in detail elsewhere. <sup>10-11</sup> Therefore, here we

focus only on the rate-limiting TSs for  $H^+GAG$  decompositions. Starting from the  $[O^{1\tau}]$ -ctgttttt GM, the energized  $H^+GGA$  molecules undergo rearrangement that transfers the proton to  $N^3$ , at which point it passes through  $TS([N^3]$ -ctgctgtt $\{O^2C\sim N^3\}$ ), shown in Figure 3. The peptide bond between  $O^2C$  and  $N^3$  is cleaved simultaneously as the  $O^1$ - $CO^2$  bond of the oxazolone ring is formed.  $TS[N^3]$ -ctgctgtt $\{O^2C\sim N^3\}$  lies below the lowest energy product asymptote,  $[b_2]^+$   $(H^+AMOx) + A$ , by 37 - 63 kJ/mol, with  $[y_1 + 2H]^+$   $(H^+A) + AMOx$  products another 6 - 12 kJ/mol higher, Figure 3. Thus, the formation of  $[b_2]^+$  and  $[y_1 + 2H]^+$  ions is limited by the energies of the separated products, i.e., they have loose TSs. This conclusion is consistent with the large cross sections observed for both  $[b_2]^+$  and  $[y_1 + 2H]^+$ , Figure 1. Formation of  $[b_2]^+ + A$  is calculated to lie 157 - 179 kJ/mol above the GM and  $[y_1 + 2H]^+ + AMOx$  is 169 - 190 kJ/mol above the GM, Supporting Table S2.

# Further dissociation of $[b_2]^+$ to $[a_2]^+$

The mechanism for dissociation of H<sup>+</sup>AMOx ([b<sub>2</sub>]<sup>+</sup>) by decarbonylation to form [a<sub>2</sub>]<sup>+</sup> has been detailed previously.<sup>32</sup> This reaction passes over a TTS, TS(H<sup>+</sup>AMOx[N<sup>2</sup>]-c{OC~O}) (also located by Siu and co-workers),<sup>27</sup> lying 126 – 138 kJ/mol above the [b<sub>2</sub>]<sup>+</sup> product and 289 - 315 kJ/mol above the H<sup>+</sup>GGA GM. A second similar TTS, TS(H<sup>+</sup>AMOx[N<sup>1</sup>]-c{OC~O}), lies 20 – 24 kJ/mol higher than the [N<sup>2</sup>] analogue, Table S3. These form an acyclic C<sub>3</sub>H<sub>7</sub>N<sub>2</sub>O<sup>+</sup> [a<sub>2</sub>]<sup>+</sup> product ion and CO. This acyclic product can cyclize to a lower energy form, but this requires passing over a barrier higher than TS(H<sup>+</sup>AMOx[N<sup>2</sup>]-c{OC~O}), a mechanism explored by Siu and co-workers.<sup>27</sup>

# Further dissociation of $[y_1 + 2H]^+$ to $CH_3CHNH_2^+$ (m/z 44)

The  $[y_1 + 2H]^+$  (H<sup>+</sup>A) product can further dissociate by loss of H<sub>2</sub>O + CO to form CH<sub>3</sub>CHNH<sub>2</sub><sup>+</sup> (m/z 44) in reaction 7. Starting from  $[y_1 + 2H]^+$  (H<sup>+</sup>A), water loss occurs via TS([N<sup>3</sup>-O<sup>4</sup>]-c{CC~O<sup>4</sup>H<sub>2</sub>}), Figure 3. This process involves the transfer of a proton from [N<sup>3</sup>] to  $[O^4]$  and a concerted cleavage of the CC-O<sup>4</sup>H<sub>2</sub> bond resulting in water formation. The resulting

intermediate (CH<sub>3</sub>CHNH<sub>2</sub>CO[N<sup>3</sup>]-c)(H<sub>2</sub>O<sub>HN</sub>), Table S2, in which the water oxygen bonds to the amine hydrogen, undergoes further loss of CO via TS(CH<sub>3</sub>CHNH<sub>2</sub>CO[N<sup>3</sup>]-c{C $\sim$ CO<sup>3</sup>})(H<sub>2</sub>O<sub>HN</sub>), which involves cleavage of the C-CO<sup>3</sup> bond, Figure 3 and Table S3. The tight TS([N<sup>3</sup>-O<sup>4</sup>]-c{CC $\sim$ O<sup>4</sup>H<sub>2</sub>}) lies 310 – 336 kJ/mol above the GM and 9 – 29 kJ/mol above (9 kJ/mol below at M06-2X) the TS for CO loss. The products CH<sub>3</sub>CHNH<sub>2</sub><sup>+</sup> (m/z 44) + H<sub>2</sub>O + CO + AMOx, are calculated to lie 27 – 57 kJ/mol below the rate-limiting TS and 84 – 114 kJ/mol above the [y<sub>1</sub> + 2H]<sup>+</sup> (H<sup>+</sup>A) + AMOx products. Thus, the formation of CH<sub>3</sub>CHNH<sub>2</sub><sup>+</sup> (m/z 44) + CO + H<sub>2</sub>O + AMOx is limited by the TTS for water loss from H<sup>+</sup>A, TS([N<sup>3</sup>-O<sup>4</sup>]-c{CC $\sim$ O<sup>4</sup>H<sub>2</sub>}).

### $[y_2 + 2H]^+/[a_1]^+$ Formation

Primary dissociation of H<sup>+</sup>GGA to [y<sub>2</sub> + 2H]<sup>+</sup> (H<sup>+</sup>GA) + CO + CH<sub>2</sub>NH (reaction 4) and  $[a_1]^+$  (CH<sub>2</sub>NH<sub>2</sub><sup>+</sup>) + CO + GA (reaction 5a) must involve transfer of the mobile proton to the N<sup>2</sup> amide nitrogen and subsequent loss of CO. We found three TSs for this decarbonylation reaction (Supporting Figure S2):  $TS([N^2]-ttgttttt\{N^1C\sim CO^1\sim N^2C\})$ , Figure 3, is the lowest of these at all  $TS([N^2]-ctgttttt\{N^1C\sim CO^1\sim N^2C\})$ along  $TS([N^2]$ levels of theory, with and cgcttttt{N¹C~CO¹~N²C}). These three TSs have very similar energies of 166 – 177, 168 – 181, and 169 – 181 kJ/mol above the GM, respectively, Supporting Table S3. These TSs differ from each other only in the spatial arrangement of the incipient immonium ion. We also tried to find a pathway that involves direct dissociation to  $[y_2 + 2H]^+$  and  $[a_1]^+$  ions and not a sequential dissociation via CO loss but were unable to do so. The TSs found here are analogous to the ones found for the loss of CO from H<sup>+</sup>GG,<sup>37</sup> H<sup>+</sup>GGG,<sup>10</sup> H<sup>+</sup>GAG,<sup>11</sup> and H<sup>+</sup>AGG.<sup>38</sup>

This decarbonylation reaction forms the proton-bound dimer (CH<sub>2</sub>NH)H<sup>+</sup>(GA), which easily dissociates to form either  $[y_2 + 2H]^+$  (H<sup>+</sup>GA) + CH<sub>2</sub>NH in reaction 4 or  $[a_1]^+$  (CH<sub>2</sub>NH<sub>2</sub><sup>+</sup>) + GA in reaction 5a, Figure 3. Both of these channels are limited by their separated product energies, which is consistent with the large cross sections observed for these channels, Figure 1. Formation of  $[y_2 + 2H]^+$  + CH<sub>2</sub>NH + CO is found to be 5 – 33 kJ/mol above the rate-limiting TSs, whereas  $[a_1]^+$  + GA + CO lies 64 – 96 kJ/mol above the rate-limiting TSs and 56 – 72 kJ/mol above the

competing  $[y_2 + 2H]^+$  channel, Tables S2 and S3. These two reactions compete directly because the proton is shared between the two molecules at their favored protonation sites.

In the previous work on H<sup>+</sup>GGG and H<sup>+</sup>GAG,<sup>10-11</sup> the initial decarbonylation reaction also yielded a subsequent product corresponding to combined CO + NH<sub>3</sub> loss. These channels pass over a TTS and hence yield small cross sections. In the present system, the analogous channel is apparently sufficiently inefficient that the product ion at m/z 159 could not be resolved from the m/z 158 product,  $\lceil a_3 \rceil^+$ .

Further dissociation of  $[y_2 + 2H]^+$  to  $[y_1 + 2H]^+_{HE}$ 

The  $[y_2 + 2H]^+$  product can further dissociate to  $[y_1 + 2H]^+$  (H<sup>+</sup>A) in reaction 2b via a TTS, TS([N³]-tt{N²C~CO²~N³C}), Figure 3, which involves a concerted cleavage of the N²C-CO² and O²C-N³C bonds, resulting in the loss of CO and CH<sub>2</sub>NH. This TS lies 328 – 369 kJ/mol above the GM and 161 – 192 kJ/mol above the TTS for CO loss that leads to  $[y_2 + 2H]^+$  formation, Supporting Table S3. Formation of  $[y_1 + 2H]^+_{HE}$  (H<sup>+</sup>A) + 2CO + 2CH<sub>2</sub>NH is calculated to lie 12 – 39 kJ/mol above TS([N³]-tt{N²C~CO²~N³C}), 167 – 193 kJ/mol above the  $[y_2 + 2H]^+$  + CO + CH<sub>2</sub>NH products, and 171 – 212 kJ/mol above the  $[y_1 + 2H]^+$  + AMOx products. Thus the formation of  $[y_1 + 2H]^+_{HE}$  is limited by its product energies at all levels of theory, which is consistent with its large cross section (Figure 1). The formation of  $[y_1 + 2H]^+_{HE}$  competes with formation of  $[a_1]^+$  (CH<sub>2</sub>NH<sub>2</sub><sup>+</sup>) in reaction 5b. This product channel lies 49 – 76 kJ/mol above the TTS and 33 – 46 kJ/mol *above* the competing  $[y_1 + 2H]^+_{HE}$  product, Tables S2 and S3. Thus, its cross section is likely to be smaller than that for  $[y_1 + 2H]^+_{HE}$ , which suggests reaction 5a dominates the production of  $[a_1]^+$  in Figure 1.

### $[b_3]^+$ Formation (Loss of Water from $H^+GGA$ )

Loss of water from H<sup>+</sup>GGA can occur via a mechanism similar to that found for H<sup>+</sup>GGG and H<sup>+</sup>GAG <sup>10-11</sup>. This occurs by transfer of a proton to the C-terminal hydroxyl group, O<sup>4</sup>H, and subsequent ring formation over the rate-limiting tight TS([O<sup>1t</sup>-O<sup>4</sup>]-ctgtt{C~O<sup>4</sup>H}), Figure 3. This

TTS lies 103 - 128 kJ/mol above the GM, and forms a complex of water and protonated 2-glycylaminomethyl-(4-methyl-5-oxazolone), H<sup>+</sup>GAMMOx[N<sup>3</sup>], which lies 71-87 kJ/mol above the GM and 29 - 44 kJ/mol below the TTS, Tables S2 and S3. This complex, (H<sup>+</sup>GAMMOx[N<sup>3</sup>]-ctgtt)(H<sub>2</sub>O<sub>CO1</sub>-HO,CH-OH), where the water hydrogen bonds to O<sup>1</sup>C and the methyl group, can lose water via a loose TS to form the final products, Figure 3, which lie 97 - 117 kJ/mol above the GM and 5-25 kJ/mol *below* the TTS. Even though calculations indicate that water loss is lower in energy than [b<sub>2</sub>]<sup>+</sup> formation by 60-78 kJ/mol, because the [b<sub>3</sub>]<sup>+</sup> channel is limited by a TTS, it does not compete effectively with the pathways having loose TSs, explaining its small cross section in Figure 1.

We had also located alternative pathways for water loss in the H<sup>+</sup>GGG and H<sup>+</sup>GAG studies  $^{10\text{-}11}$ . The analogous TS for H<sup>+</sup>GGA occurs by transfer of a proton from the N<sup>2</sup> nitrogen to the terminal hydroxyl group via TS([N<sup>2</sup>-O<sup>4</sup>]-(tg)tg(tg){C $\sim$ O<sup>4</sup>H}), Supporting Figure S2. The constrained head-to-tail cyclic geometry of this TS not only raises its energy (189 – 218 kJ/mol above GM and 78 – 95 kJ/mol above TS[O<sup>1t</sup>-O<sup>4</sup>]) but also makes it entropically less favored.

The  $[b_3]^+$  fragment ion can also be a nine-membered ring structure, as located for other peptides,  $^{10, 45}$  but this  $[b_3]^+$  product was found to be much higher in energy (by 90 kJ/mol for H<sup>+</sup>AAAAR, and 69 - 85 kJ/mol for H<sup>+</sup>GGG) than the non-cyclic  $[b_3]^+$  oxazolone product in these studies. Thus, we have not investigated this pathway further here.

# Further dissociation of $[b_3]^+$ to $[a_3]^+$

Decomposition of  $[b_3]^+$  to lose CO can occur in the presence and absence of the water product, where the former is lower in energy. In the H<sup>+</sup>GGG study, we found that although loss of CO from  $[b_3]^+$  in the presence of water is energetically favored, the TS for this process is well above the loose TS associated with the  $[b_3]^+$  + H<sub>2</sub>O products. Thus, the decomposition of  $[b_3]^+$  to  $[a_3]^+$  should occur after water is lost and therefore, the pathway in which water is retained has not been examined here. Decarbonylation of  $[b_3]^+$  to form the  $[a_3]^+$  + CO products is limited by TS(H<sup>+</sup>GAMMOx[N<sup>3</sup>]-ctg(cg){C~CO<sup>3</sup>}), Figure 3, which lies 218 – 243 kJ/mol above the GM and

53 - 70 kJ/mol above the products, GGNHCHCH<sub>3</sub>[N<sup>3</sup>]<sup>+</sup>-ctgg + H<sub>2</sub>O + CO (Figure 3 and Tables S2 and S3). Here, the small magnitude of [a<sub>3</sub>]<sup>+</sup> (Figure 1) is mainly determined by the cross section of its precursor, [b<sub>3</sub>]<sup>+</sup>. Similar to the findings of this study and that for H<sup>+</sup>GGG <sup>10</sup>, Allen et al. found that formation of [a<sub>3</sub>]<sup>+</sup> from H<sup>+</sup>AAAAR was limited by a TTS and produced an acyclic imine formed by decarbonylation of the [b<sub>3</sub>]<sup>+</sup>ring.<sup>45</sup> They also found that this species could readily undergo further decomposition to yield [b<sub>2</sub>]<sup>+</sup> + CH<sub>3</sub>CH=NH. This latter process would not be observed here because of the already large [b<sub>2</sub>]<sup>+</sup> ion signal from reaction 1.

In the H<sup>+</sup>GGG and H<sup>+</sup>GAG studies,<sup>10-11</sup> we had also explored the cyclization of the [a<sub>3</sub>]<sup>+</sup> ion and found that the rate-limiting TS for cyclization was above the rate-limiting TS of the decarbonylation step. Thus, the acyclic [a<sub>3</sub>]<sup>+</sup> product, GGNHCHCH<sub>3</sub><sup>+</sup>[N<sup>3</sup>], should be formed at the experimental threshold; however, cyclization may occur at higher energies, although it is an entropically disfavored process. As a result, the cyclization pathway of the [a<sub>3</sub>]<sup>+</sup> product from H<sup>+</sup>GGA was not explicitly examined.

### Analysis of Primary Dissociation Channels

Scheme 1 outlines the relationships between reactions 1 - 8 on the basis of the reaction mechanisms calculated here and previous work.  $^{32}$  The primary dissociations from H<sup>+</sup>GGA are the formation of  $[b_2]^+$  in reaction 1, production of  $[y_1 + 2H]^+$  in reaction 2a, loss of water to form  $[b_3]^+$  in reaction 3, and loss of CO, which rapidly leads to the formation of  $[y_2 + 2H]^+$  in reaction 4, and  $[a_1]^+$  in reaction 5a. Formations of  $[b_2]^+$  and  $[y_1 + 2H]^+$  are limited by the asymptotic energy of their products, whereas the formation of  $[b_3]^+$  and loss of CO are limited by TTSs, TS( $[O^{1t}-O^4]-ctgtt\{C\sim O^4H\}$ ) and TS( $[N^2]-ttgttttt\{N^1C\sim CO^1\sim N^2C\}$ ), respectively. For the two channels initiated by CO loss over TS( $[N^2]-ttgttttt\{N^1C\sim CO^1\sim N^2C\}$ ), formation of  $[y_2 + 2H]^+$  and  $[a_1]^+$  products lie at higher energies and thus have loose TSs. The loose TSs of  $[b_2]^+$ ,  $[y_1 + 2H]^+$ ,  $[y_2 + 2H]^+$ , and  $[a_1]^+$  are consistent with the relatively large magnitudes of their cross sections, whereas the TTS of  $[b_3]^+$  is consistent with its small cross section in Figure 1. As mentioned earlier, the primary product for CO loss (m/z 176) was not observed, which given the mechanisms elucidated above,

implies that the CO loss product decomposes rapidly when the thresholds for its subsequent decompositions are reached. Because loss of CO over a TTS competes with the loose TS for the dominant  $[b_2]^+$  and  $[y_1 + 2H]^+$  products at a similar energy, the m/z 176 cross section apparently never reaches an appreciable magnitude until after this intermediate can begin to dissociate further. This conclusion is similar to those reached in our previous studies with H<sup>+</sup>GGG and H<sup>+</sup>GAG. 10-11

These interrelated processes have been analyzed by summing the cross sections of the sequential channels with their precursor channels to form composite channels: m/z 115 + m/z 87 ( $[b_2]^+ + [a_2]^+ = [b_2]^+_{tot}$ ), m/z 90 + m/z 44 ( $[y_1 + 2H]^+ + CH_3CHNH_2^+ = [y_1 + 2H]^+_{tot}$ ), m/z 147 + m/z 90 ( $[y_2 + 2H]^+ + [y_1 + 2H]^+_{HE} = [y_2 + 2H]^+_{tot}$ ), and m/z 186 + m/z 158 ( $[b_3]^+ + [a_3]^+ = [b_3]^+_{tot}$ ). The  $[y_1 + 2H]^+_{HE}$  cross section was isolated by subtracting the model for the low-energy (LE) portion of  $[y_1 + 2H]^+$  from the total  $[y_1 + 2H]^+$  cross section. In all cases, the composite cross sections change smoothly with energy, consistent with the assigned sequential dissociations.

Zero-pressure extrapolated cross sections (rigorously single collision conditions) were analyzed only for the four major primary product channels:  $[b_2]^+_{tot}$ ,  $[y_1 + 2H]^+_{tot}$ ,  $[y_2 + 2H]^+_{tot}$ , and  $[a_1]^+$ . The smaller cross section of the  $[b_3]^+$  product could not be extrapolated to zero-pressure conditions with accuracy and was therefore analyzed using a data set taken at a medium pressure of Xe. In either case, the cross sections of the four major primary channels were modeled competitively using Supporting Eq. S1 assuming the DFT GM structure for H<sup>+</sup>GGA,  $[O^{1t}]$ -etgttttt. The shape of the large  $[b_2]^+_{tot}$  cross section defines the n parameter in Eq. S1, which also means that the  $[b_2]^+_{tot}$  threshold energy is the most accurately determined threshold energy. The model for the medium-pressure data set and all five primary products is shown in Figure 4. Table 1 lists optimized parameters of Eq. S1 for both zero and medium-pressure data sets. Thresholds obtained at medium pressure, e.g., that for the  $[b_3]^+$  product, were corrected for pressure effects as discussed in the Supporting Information. In all cases, the zero-pressure thresholds are estimated by adding  $0.29 \pm 0.04$  eV to the medium-pressure threshold, the average shift observed for the four major primary channels with zero-pressure cross sections that could be directly modeled. This procedure yielded 0 K threshold energies for the zero-pressure extrapolated data for the five primary

processes of  $1.91 \pm 0.05$  [b<sub>2</sub>]<sup>+</sup>,  $1.88 \pm 0.06$  [y<sub>1</sub> + 2H]<sup>+</sup>,  $1.57 \pm 0.06$  [b<sub>3</sub>]<sup>+</sup>,  $2.31 \pm 0.05$  [y<sub>2</sub> + 2H]<sup>+</sup>, and  $2.67 \pm 0.05$  eV [a<sub>1</sub>]<sup>+</sup>. All of these competitive products were also analyzed assuming that the reaction begins at the MP2 GM of H<sup>+</sup>GGA, [N<sup>1</sup>]-ttggtgtt. This change resulted in an upward shift in all thresholds of only 0.03 eV. Our best set of threshold energies is the average of these two interpretations with uncertainties that include these deviations, as reported in Table 2.

As discussed in the Supporting Information, analysis of the  $[y_2 + 2H]^+_{tot}$  and  $[a_1]^+$  cross sections is not straightforward because theory indicates that these two channels result from sequential decompositions from a product ion formed by CO loss, which was not observed, Figure 1. This led us to analyze these two cross sections using two models: T<sub>P</sub>L<sub>P</sub>L<sub>P</sub> and T<sub>P</sub>L<sub>S</sub>L<sub>S</sub>, where T (tight) and L (loose) list the TSs used for CO loss,  $[y_2 + 2H]^+$ , and  $[a_1]^+$ , respectively, and the subscripts indicate treatment as a primary (P) or secondary (S) reaction. Details of the analysis using the T<sub>P</sub>L<sub>S</sub>L<sub>S</sub> model (which requires extensive frequency scaling) can be found in the Supporting Information, because the discussion there indicates that the best analysis of the [y<sub>2</sub> + 2H]<sup>+</sup> and  $[a_1]$ <sup>+</sup> products is obtained by the  $T_PL_PL_P$  approach. Indeed, the  $T_PL_PL_P$  model reproduces the five competing cross sections well, reproducing all the cross sections to about 5 eV, Figure 4. A similar conclusion was reached in our previous studies of H<sup>+</sup>GGG and H<sup>+</sup>GAG.<sup>10-11</sup> Treating the formation of  $[y_2 + 2H]^+$  and  $[a_1]^+$  as primary products  $(T_PL_PL_P)$  may shift the thresholds upwards somewhat because the possibility that the initial CO product takes away energy is not accounted for and the dissociation is treated as occurring to one ion and one neutral (taken to be a loose complex of the two neutral species). In our previous analogous studies, reasonable thermochemistry was still obtained from this model although these two thresholds are conservatively listed as upper limits here.

As shown in Figure 4, the  $T_PL_PL_P$  model fits the  $[b_2]^+$  and  $[a_1]^+$  cross-sections well without the use of any cross section scaling factors. In order to reproduce the  $[y_1 + 2H]^+_{tot}$  and  $[y_2 + 2H]^+_{tot}$  cross sections, their PSL frequencies below 900 cm<sup>-1</sup> needed to be scaled by  $1.10 \pm 0.01$  and  $1.29 \pm 0.01$ , respectively, which indicates a tighter TS than calculated. For  $[y_2 + 2H]^+_{tot}$ , this scaling can be attributed to the inability to properly treat the initial CO loss, which is inhibited by a TTS. For

the  $[y_1 + 2H]^+$  cross section, this scaling is needed in order to properly capture the decline in the cross section above its peak near 2.5 eV, a consequence of competition with the  $[b_2]^+$  product ion. In order to accurately reproduce reaction 3 forming  $[b_3]^+$  in the competitive modeling, Figure 4, the TTS frequencies below 900 cm<sup>-1</sup> needed to be scaled by 0.77 ± 0.01. The need for this modest scaling of the vibrational frequencies indicates that the TTS for  $[b_3]^+$  is looser than suggested by theory, as similarly found for H<sup>+</sup>GGG (0.79 ± 0.01) and H<sup>+</sup>GAG (0.70 ± 0.02). <sup>10-11</sup> Even with this scaling, the  $[b_3]^+$  cross section is not reproduced with complete fidelity, which probably indicates that competition with other channels, both at threshold and higher energies, is not accurately modeled.

### Analysis of Secondary Dissociation Channels

Once the fitting parameters for the five primary channels were determined, sequential dissociation channels of  $[a_2]^+$  from  $[b_2]^+$ ,  $[y_1 + 2H]^+_{HE}$  from  $[y_2 + 2H]^+$ , m/z 44 ( $[y_1 + 2H - CO - H_2O]^+$ ) from  $[y_1 + 2H]^+$ , and  $[a_3]^+$  from  $[b_3]^+$  in reactions 6, 2b, 7, and 8 were analyzed. In all of these sequential analyses, threshold energies of all five competing primary channels were the same as those obtained when the secondary channels were not included.

The dissociation of the  $[b_2]^+$  ion to form  $[a_2]^+$  in reaction 6 occurs by the TTS, TS(H<sup>+</sup>AMOx[N<sup>2</sup>]-c{OC~O}), as previously calculated by Armentrout and Clark<sup>32</sup> and similar to that outlined previously by El Aribi et al.<sup>27</sup> This analysis required scaling of the  $[a_2]^+$  cross section (compare  $\sigma_0$  values in Table 1), which is similar to the  $[a_2]^+$  analysis in the H<sup>+</sup>GGG and H<sup>+</sup>GAG studies,  $^{10-11}$  Figure 5a. The need for scaling in these three peptide systems differs from Armentrout and Clark's  $^{32}$  analysis of the primary  $[b_2]^+ \rightarrow [a_2]^+$  process where no scaling was required. This discrepancy indicates that the statistical assumptions used to estimate energy deposition for the sequential process may not be completely accurate. The sequential dissociation model reproduces the entire  $[a_2]^+$  cross section as well as the decline in the  $[b_2]^+$  cross section, Figure 5a. We find the threshold energy of the  $[a_2]^+$  product when formed in reaction 6 is 3.24  $\pm$  0.09 eV at medium pressure (Table 1). This threshold lies 1.59  $\pm$  0.13 eV above the threshold for  $[b_2]^+$ , in excellent

agreement with the threshold energy of  $1.57 \pm 0.12$  eV measured for direct dissociation of the  $[b_2]^+$  reactant ion to  $[a_2]^+$  by Armentrout and Clark.<sup>32</sup>

The dissociation of  $[y_2 + 2H]^+$  (m/z 147) to form  $[y_1 + 2H]^+_{HE}$  (m/z 90) in reaction 2b occurs via a PSL TS. Here the sequential dissociation of  $[y_2 + 2H]^+$  to  $[y_1 + 2H]^+_{HE}$  required slight scaling of the  $[y_1 + 2H]^+_{HE}$  cross section and reproduces the  $[y_1 + 2H]^+_{HE}$  cross section up to  $\sim 6.5$  eV, Figure 5b, yielding a threshold energy of  $4.91 \pm 0.08$  eV at medium pressure. This threshold lies  $2.93 \pm 0.11$  eV above the threshold of  $[y_2 + 2H]^+$ . We also analyzed the  $[y_1 + 2H]^+_{HE}$  (m/z 90) using the TTS, ( $[N^3]$ -tt{ $N^2C\sim CO^2\sim N^3C$ }), because even though the TTS is calculated to lie 12 - 39 kJ/mol below the  $[y_1 + 2H]^+ + 2$  CO + 2 CH<sub>2</sub>NH asymptote, it may be close enough in energy that it controls this pathway. This approach results in a much larger kinetic shift and a threshold energy of  $4.19 \pm 0.12$  eV at medium pressure, which lies  $2.21 \pm 0.14$  eV above the threshold of  $[y_2 + 2H]^+$ . This analysis yields a model virtually identical to that shown in Figure 5b. As for the  $[y_2 + 2H]^+$  product, these thresholds are considered upper limits because they do not account for energy removed by the initial decarbonylation.

The dissociation of  $[y_1 + 2H]^+$  to form m/z 44 in reaction 7 occurs via the tight TS( $[N^3-O^4]$ -c $\{CC\sim O^4H\}$ ). This sequential dissociation analysis reproduced the low-energy portion (up to  $\sim 5.5 \text{ eV}$ ) of the m/z 44 cross section requiring slight scaling of its cross section scaling, Figure 5c, yielding a threshold energy of  $2.78 \pm 0.05 \text{ eV}$  at medium pressure. At higher energies (above  $\sim 5.5 \text{ eV}$ ), the m/z 44 cross section can also be formed from decomposition of  $[y_1 + 2H]^+_{HE}$ . Because this process is a third-order dissociation, it cannot be analyzed currently because it is difficult to define all energy distributions (internal and translational for all products) for such high-order dissociations.

The dissociation of  $[b_3]^+$  to form  $[a_3]^+$  in reaction 8 takes place by loss of CO. Similar to its  $[b_3]^+$  precursor, the  $[a_3]^+$  fragment has weak intensity, which leads to zero-pressure extrapolated cross sections that were of insufficient quality to model with confidence. Therefore, we have analyzed the  $[a_3]^+$  cross section acquired at medium pressure of xenon to obtain a threshold of 2.19  $\pm$  0.04 eV. The  $[a_3]^+$  cross section was analyzed as a sequential product of  $[b_3]^+$  while still retaining

the competition with the five primary channels and required slight scaling of its cross section, Figure 5d. Fitting parameters of this channel obtained from the analysis of medium-pressure data are listed in Table 1.

### Comparison between Theoretical and Experimental Energetics

Figures 4 and 5a-d show that the experimental cross sections for reactions 1 - 8 can be reproduced well by Supporting Eqs. S1, S3a, and S3b over a wide range of energies (up to 4 –6 eV) and over two orders of magnitude in cross section. As further validation of the reaction mechanisms and energetics, we also compare the experimental threshold energies to calculated threshold energies. These comparisons are shown in Table 2 and Figure 6. When only the five primary products are considered, mean absolute deviations (MADs) between theory and experiment range between 13 and 27 kJ/mol for all four levels of theory, comparable to 10 - 21for H<sup>+</sup>GAG and 6 – 14 for H<sup>+</sup>GGG. <sup>10-11</sup> Among the primary products, the largest deviations are those for reactions 3 ( $[b_3]^+$ ) and 4 ( $[y_2 + 2H]^+$ ), where theory underestimates the threshold energies by 25 - 50 and 19 - 51 kJ/mol, respectively. As noted above, our modeling for reaction 4 ([y<sub>2</sub> + 2H]<sup>+</sup>) is speculative because theory indicates its formation involves dissociation to three molecular species (one ion and two neutrals), whereas our best modeling assumes  $[y_2 + 2H]^+$  is formed as a primary product (T<sub>P</sub>L<sub>P</sub>L<sub>P</sub> model). This modeling approach may overestimate the true threshold energy because competition between the other primary products and the TTS for CO loss is not adequately represented. In fact, the deviations obtained for  $[y_2 + 2H]^+$  are similar to those obtained for the analogous product from H<sup>+</sup>GGG (13 – 46 kJ/mol) <sup>10</sup> and H<sup>+</sup>GAG (9 – 45 kJ/mol) <sup>11</sup> where the same issue in analysis was encountered. For the [b<sub>3</sub>]<sup>+</sup> cross section, analysis is made challenging by the fact it has the smallest cross section. If only thresholds for  $[b_2]^+$ ,  $[y_1 +$ 2H]<sup>+</sup>, and  $[a_1]$ <sup>+</sup> are considered, the MADs drop to  $18 \pm 9$  (B3LYP),  $6 \pm 2$  (B3LYP-D3),  $8 \pm 7$ (MP2), and  $6 \pm 3$  (M06-2X) kJ/mol.

For the [a<sub>2</sub>]<sup>+</sup> secondary product, the threshold obtained here lies within experimental uncertainty of two previous measurements, Table 2. The most accurate of these comes from the

direct examination of the decomposition of  $[b_2]^+$  to  $[a_2]^+$  by Armentrout and Clark.<sup>32</sup> These experimental values are in reasonable agreement with most levels of theory except MP2 and particularly B3LYP are somewhat low. This is also true for thresholds predicted for the  $[a_3]^+$  secondary product. For  $[y_1 + 2H]^+_{HE}$ , all levels of theory are consistent with the upper limits determined experimentally for this secondary channel. The experimental threshold for the  $CH_3CHNH_2^+$  (m/z 44) secondary product is the only channel where the experimental value is lower than predicted by theory, and therefore this value agrees best with the B3LYP prediction. If the thermochemistry for eight fragmentations from  $H^+GGA$  (excluding the  $[y_1 + 2H]^+_{HE}$  channel) is considered, the MADs increase slightly to 17 - 27 kJ/mol (Table 2). This overall comparison is similar to our previous results for  $H^+GGG$  and  $H^+GAG$ .<sup>10-11</sup> If the  $[y_1 + 2H]^+_{HE}$  thresholds are also included, the MADs increase to 22 - 36 kJ/mol when using the TTS analysis and 27 - 42 kJ/mol when using the PSL TS analysis, with the measured values agreeing best with the M06-2X prediction.

Overall, the B3LYP-D3 and M06-2X levels of theory give the best agreement with experiment, with deviations for MP2 being slightly higher and those for B3LYP being about twice as high. Thus, reasonable agreement between experiment and theory is obtained for most reaction channels, which in turn validates the reaction mechanisms described above.

#### Comparison of $H^+GGA$ to $H^+GGG$ and $H^+GAG$ decomposition

Figure 7 compares the absolute cross sections of the total, the primary products,  $[b_2]^+$ ,  $[y_1 + 2H]^+$ ,  $[y_2 + 2H]^+$ ,  $[a_1]^+$ ,  $[b_3]^+$ , and the secondary product,  $[a_2]^+$  observed in the decomposition of the three protonated tripeptides,  $H^+GGA$  (present work),  $H^+GGG$ , and  $H^+GAG$ , obtained on the same instrument to investigate the effect of the change in the amino acid sequence. As shown in Figure 7a, the total cross sections of all three tripeptides are very similar, with that for  $H^+GAG$  being slightly larger than that for  $H^+GGG$  and that for  $H^+GGA$  being slightly smaller. This behavior tracks with the  $[b_2]^+$  product ion, the dominant primary product with the largest cross section at low energies for all three tripeptides, Figure 7b. This product is  $H^+AMOx$  for both

H<sup>+</sup>GGA and H<sup>+</sup>GGG, but methylated, H<sup>+</sup>AMMOx, for H<sup>+</sup>GAG. This methylation stabilizes the formation of  $[b_2]^+$  from H<sup>+</sup>GAG, such that its threshold energy is  $11 \pm 15$  kJ/mol (8 – 12 kJ/mol according to theory) below that for H<sup>+</sup>GGG. The threshold for  $[b_2]^+$  from H<sup>+</sup>GGA is another  $15 \pm 8$  kJ/mol higher (4 – 7 kJ/mol, theory), a consequence of the more severe competition with the  $[y_1 + 2H]^+$  product, as evident in Figure 7b. This also explains why the  $[b_2]^+$  cross section for H<sup>+</sup>GGA is smaller than those for H<sup>+</sup>GGG and H<sup>+</sup>GAG. For the secondary  $[a_2]^+$  product, Figure 7b, the cross section from H<sup>+</sup>GAG is larger because it has a larger precursor  $[b_2]^+$  cross section and a lower threshold (by  $54 \pm 10$  kJ/mol) than that for H<sup>+</sup>GGG. This is because both the  $[b_2]^+$  and subsequent  $[a_2]^+$  product ions are methylated. In contrast, the  $[a_2]^+$  cross section is slightly smaller for H<sup>+</sup>GGA compared to H<sup>+</sup>GGG, which mainly reflects the differences in the magnitude of the  $[b_2]^+$  precursor cross section, as the threshold energy of  $[a_2]^+$  is same for both H<sup>+</sup>GGG and H<sup>+</sup>GGA because the  $[b_2]^+$  (H<sup>+</sup>AMOx) precursor is the same for these two tripeptides.

Methylation in H<sup>+</sup>GGA stabilizes the  $[y_1 + 2H]^+$  product, H<sup>+</sup>A, compared to the  $[y_1 + 2H]^+$  (H<sup>+</sup>G) product from H<sup>+</sup>GGG and H<sup>+</sup>GAG. Indeed, alanine has a higher proton affinity (894.5 – 902.4 kJ/mol compared to glycine (880.7 – 886.6 kJ/mol). Here expectations are in agreement with a lower threshold energy for  $[y_1 + 2H]^+$  from H<sup>+</sup>GGA by 9 ± 12 (15 – 36 theory) and 1 ± 9 (7 – 13 theory) kJ/mol compared to H<sup>+</sup>GAG and H<sup>+</sup>GGG, respectively. Indeed, these trends in threshold energies explain the large change in cross section magnitudes for the  $[y_1 + 2H]^+$  product.

As shown in Figure 7c, the  $[y_2 + 2H]^+$  products of the three peptides vary somewhat in magnitude and apparent threshold with H<sup>+</sup>GG from H<sup>+</sup>GGG being the largest and H<sup>+</sup>AG from H<sup>+</sup>GAG being the smallest. In contrast, analyses of these data indicates that they all have similar thresholds within  $11 \pm 17$  kJ/mol, in agreement with theory, which places them within 5 - 8 kJ/mol of one another. Thus, most of the variation can be attributed to competition of the primary  $[y_2 + 2H]^+$  product with  $[b_2]^+$  and  $[y_1 + 2H]^+$ . This variation in magnitude also influences the  $[y_1 + 2H]^+$ HE product, which is formed in both H<sup>+</sup>GGA and H<sup>+</sup>GGG, leading to the second feature at high energies, Figure 7b. In both systems, the primary  $[y_2 + 2H]^+$  product decomposes by loss of CO and CH<sub>2</sub>NH to yield  $[y_1 + 2H]^+$ HE. Because the cross section of the precursor  $[y_2 + 2H]^+$  is

smaller in H<sup>+</sup>GGA compared to H<sup>+</sup>GGG, the absolute cross section of the  $[y_1 + 2H]^+_{HE}$  is also smaller. The high-energy feature in H<sup>+</sup>GGG is clearly much more obvious in the H<sup>+</sup>GGG system because of the small size of the primary  $[y_1 + 2H]^+$  cross section. In the H<sup>+</sup>GAG system, the  $[y_2 + 2H]^+$  product also decomposes at higher energies via an analogous process, but now the favored product channel is CH<sub>3</sub>CHNH<sub>2</sub><sup>+</sup> (m/z 44) + CO + G, rather than CH<sub>3</sub>CHNH + CO +  $[y_1 + 2H]^+$  (H<sup>+</sup>G).

Competition of  $[a_1]^+$  with  $[y_2 + 2H]^+$  is expected to influence its absolute cross section and energetics. In fact, the  $[a_1]^+$  products of all three tripeptides follow the same trend as the  $[y_2 + 2H]^+$  products. The increase from H<sup>+</sup>GGA to H<sup>+</sup>GGG is consistent with an increase in the threshold energy by  $11 \pm 9$  (4 theory) kJ/mol. Also following the  $[y_2 + 2H]^+$  trend, the H<sup>+</sup>GGA  $[a_1]^+$  has a slightly larger cross section than the H<sup>+</sup>GAG system.

Methylation also has an effect on the cross section and energetics of the water loss product,  $[b_3]^+$ . Here, the methyl group on the C-terminal residue in H<sup>+</sup>GGA has a more pronounced affect than methylation of the middle residue in H<sup>+</sup>GAG as we find that the  $[b_3]^+$  H<sup>+</sup>GAMMOx product from H<sup>+</sup>GGA has a larger cross section than the comparable product from H<sup>+</sup>GAG and H<sup>+</sup>GGG. This can be attributed to the higher threshold for  $[b_2]^+$  in H<sup>+</sup>GGA, which permits the lower energy  $[b_3]^+$  formation to compete more effectively than in the other two systems. Oddly, despite having a larger cross section, the threshold energy measured here for  $[b_3]^+$  is shifted to higher energies,  $17 \pm 11$  kJ/mol and  $6 \pm 13$  kJ/mol higher than H<sup>+</sup>GGG and H<sup>+</sup>GAG, respectively. This contrasts with theoretical predictions that lower the H<sup>+</sup>GGA  $[b_3]^+$  threshold energy by  $11 \pm 3$  kJ/mol and  $8 \pm 1$  kJ/mol compared to H<sup>+</sup>GAG and H<sup>+</sup>GGG, respectively. As noted above, the  $[b_3]^+$  threshold energy for H<sup>+</sup>GGA from theory does not agree well with the experimental value (Figure 6), whereas agreement was reasonable in the other two tripeptides. Further, the modeling of this cross section (Figure 4) is not as robust as for the other product channels, suggesting that the formation of  $[b_3]^+$  and its competition with the other channels is not described as well as desired.

### **Conclusions**

In the present study, the decomposition of protonated GGA is examined by measuring its kinetic-energy dependent collision-induced dissociation with Xe in a GIBMS. Analyses of the TCID cross sections yield 0 K threshold energies of five primary products:  $[b_2]^+$ ,  $[y_1 + 2H]^+$ ,  $[y_2 + 2H]^+$ ,  $[a_1]^+$ ,  $[b_3]^+$ , and four sequential products:  $[a_2]^+$ ,  $[a_3]^+$ ,  $[y_1 + 2H]^+_{HE}$ , and  $CH_3CHNH_2^+$  (m/z 44) after accounting for effects of reactant internal energy, multiple collisions with Xe, lifetime effects, competition among channels, and sequential dissociations. We find that these experimental threshold energies compare well with the theoretical threshold energies predicted at the B3LYP-D3 and M06-2X levels, consistent with our previous findings for H<sup>+</sup>GAG and H<sup>+</sup>GGA. Moreover the threshold energy of the sequential product,  $[a_2]^+$  is consistent with its threshold energy measured previously in our lab. Good agreement with theory also validates the reaction mechanisms described above.

The present study not only demonstrates the ability to obtain accurate thermodynamic information but also the ability to investigate the effect of a systematic change in the sequence of the tripeptide. The threshold energies of the products from H<sup>+</sup>GGA were compared to those common with H<sup>+</sup>GGG and H<sup>+</sup>GAG, to examine the effect of the slight change in the amino acid sequence. Methylation at the C-terminal amino acid, alanine in H<sup>+</sup>GGA, has a pronounced effect on the two primary products:  $[b_2]^+$  and  $[y_1 + 2H]^+$ , suppressing the cross section of the  $[b_2]^+$  channel and increasing its threshold energy. For  $[y_1 + 2H]^+$  (H<sup>+</sup>A), methylation enhances the cross section of this product while reducing its threshold energy. Methylation also affects the water loss product,  $[b_3]^+$  H<sup>+</sup>GAMMOx, yielding a larger cross section than its analogue from H<sup>+</sup>GGG and H<sup>+</sup>GAG. Overall, the present study shows that methylation has a noticeable effect on the decomposition of these simple tripeptides.

The present work can also be viewed in a broader perspective. The models shown in Figures 4 and 5 are predictions of the mass spectrum for H<sup>+</sup>GGA over a range of excitation conditions. Thus, this work and its predecessors regarding H<sup>+</sup>GGG, <sup>10</sup> H<sup>+</sup>GAG, <sup>11</sup> and H<sup>+</sup>GPA<sup>41</sup> show that accurate predictions of the mass spectrum for decomposition of small peptides can be realized. Further, the level of theory that can yield the most quantitatively valid predictions, here

M06-2X and B3LYP-GD3BJ with triple zeta basis sets, is validated and allows extension to larger peptides having with more complicated side chains. In this regard, our TCID approach coupled with IRMPD has been used to systematically explore the deamidation of protonated AspGly,<sup>51</sup> AspAla,<sup>52</sup> AspVal,<sup>53</sup> AspSer,<sup>54</sup> and AspThr,<sup>55</sup> where deamidation of asparaginyl residues in proteins is a process believed to be associated with aging. Although as yet undemonstrated, the authors believe that systems as large as a hexapeptide are probably amenable to the detailed treatment found here, although eventually, the increasing size will lead to kinetic shifts that limit the accuracy of the thermodynamic information that can be gleaned.

### Acknowledgements

The authors acknowledge support for this work by the National Science Foundation, Grant CHE-1954142, and grants of computational time from the Center for High Performance Computing (CHPC) at the University of Utah.

Electronic Supporting Information. Details of the experimental procedures and data analysis. Tables of the calculated energies of different conformers of H<sup>+</sup>GGA and its decomposition intermediates, transition states, and products. Figures showing the reaction coordinate for transcis isomerization of H<sup>+</sup>GGA, structures of key transition states and products, and modeling of the primary product cross sections using the T<sub>P</sub>L<sub>S</sub>L<sub>S</sub> model.

#### References

- 1. Chu, I. K.; Siu, C.-K.; Lau, J. K.-C.; Tang, W. K.; Mu, X.; Lai, C. K.; Guo, X.; Wang, X.; Li, N.; Xia, Y.; Kong, X.; Oh, H. B.; Ryzhov, V.; Tureček, F.; Hopkinson, A. C.; Siu, K. W. M., Proposed Nomenclature for Peptide Ion Fragmentation. *Int. J. Mass Spectrom.* **2015**, *390*, 24-27.
- 2. Roepstorff, P.; Fohlman, J., Proposal for a common nomenclature for sequence ions in mass spectra of peptides. *Biomed. Mass Spectrom.* **1984**, 11, 601.
- 3. Biemann, K., Contributions of Mass Spectrometry to Peptide and Protein Structure. *Biomed. Environ. Mass Spectrom.* **1988,** *16*, 99-111.
- 4. Becke, A. D., Density-functional Exchange Energy Approximation with Correct Asymptotic Behavior. *Phys. Rev. A* **1988**, *38*, 3098-3100.
- 5. Lee, C.; Yang, W.; Parr, R. G., Development of the Colle-Salvetti Correlation-Energy Formula into a Functional of the Electron Density. *Phys. Rev. B* **1988**, *37*, 785-789.
- 6. Grimme, S.; Antony, J.; Ehrlich, S.; Krieg, H., A Consistent and Accurate Ab Initio

- Parametrization of Density Functional Dispersion Correction (DFT-D) for the 94 Elements H-Pu. *J. Chem. Phys.* **2010**, *132*, 154104-154119.
- 7. Grimme, S.; Ehrlich, S.; Goerigk, L., Effect of the Damping Function in Dispersion Corrected Density Functional Theory. *J. Comput. Chem.* **2011**, *32*, 1456-1465.
- 8. Möller, C.; Plesset, M. S., Note on an Approximation Treatment for Many-Electron Systems. *Phys. Rev.* **1934**, *46*, 618-622.
- 9. Zhao, Y.; Truhlar, D. G., The M06 Suite of Density Functionals for Main Group Thermochemistry, Thermochemical Kinetics, Noncovalent Interactions, Excited States, and Transition Elements: Two New Functionals and Systematic Testing of Four M06-Class Functionals and 12 Other Functionals. *Theor. Chem. Acc.* **2008**, *120*, 215-241.
- 10. Mookherjee, A.; Van Stipdonk, M. J.; Armentrout, P. B., Thermodynamics and Reaction Mechanisms of Decomposition of the Simplest Protonated Tripeptide, Triglycine: A Guided Ion Beam and Computational Study. *J. Am Soc. Mass Spectrom.* **2017**, *28*, 739-757.
- 11. Mookherjee, A.; Armentrout, P. B., Thermodynamics and Reaction Mechanisms for Decomposition of a Simple Protonated Tripeptide, H<sup>+</sup>GAG: a Guided Ion Beam and Computational Study. *J. Am. Soc. Mass Spectrom.* **2019**, *30*, 1013-1027.
- 12. Ervin, K. M.; Armentrout, P. B., Translational Energy Dependence of  $Ar^+ + XY \rightarrow ArX^+ + Y$  (XY = H<sub>2</sub>, D<sub>2</sub>, HD) from Thermal to 30 eV c.m. *J. Chem. Phys.* **1985**, 83, 166-189.
- 13. Muntean, F.; Armentrout, P. B., Guided Ion Beam Study of Collision-Induced Dissociation Dynamics: Integral and Differential Cross Sections. *J. Chem. Phys.* **2001**, *115*, 1213-1228.
- 14. Moision, R. M.; Armentrout, P. B., An Electrospray Ionization Source for Thermochemical Investigation with the Guided Ion Beam Mass Spectrometer. *J. Am. Soc. Mass Spectrom.* **2007**, *18*, 1124-1134.
- 15. Ye, S. J.; Armentrout, P. B., Absolute Thermodynamic Measurements of Alkali Metal Cation Interactions with a Simple Dipeptide and Tripeptide. *J. Phys. Chem. A* **2008**, *112*, 3587-3596.
- 16. Heaton, A. L.; Armentrout, P. B., Thermodynamics and Mechanism of the Deamidation of Sodium-Bound Asparagine. *J. Am. Chem. Soc.* **2008**, *130*, 10227-10232.
- 17. Heaton, A. L.; Moision, R. M.; Armentrout, P. B., Experimental and Theoretical Studies of Sodium Cation Interactions with the Acidic Amino Acids and Their Amide Derivatives. *J. Phys. Chem. A* **2008**, *112*, 3319-3327.
- 18. Carpenter, J. E.; McNary, C. P.; Furin, A.; Sweeney, A. F.; Armentrout, P. B., How Hot are Your Ions Really? A Threshold Collision-Induced Dissociation Study of Substituted Benzylpyridinium "Thermometer" Ions. *J. Am. Soc. Mass Spectrom.* **2017**, *28*, 1876-1888.
- 19. Rodgers, M. T.; Ervin, K. M.; Armentrout, P. B., Statistical Modeling of Collision-Induced Dissociation Thresholds. *J. Chem. Phys.* **1997**, *106*, 4499-4508.
- 20. Rodgers, M. T.; Armentrout, P. B., Statistical Modeling of Competitive Threshold Collision-Induced Dissociation. *J. Chem. Phys.* **1998**, *109*, 1787-1800.
- 21. Armentrout, P. B., Statistical modeling of sequential collision-induced dissociation. *J. Chem. Phys.* **2007**, *126*, 234302.
- 22. Heaton, A. L.; Armentrout, P. B., Thermodynamics and Mechanism of Protonated Asparagine Decomposition. *J. Am. Soc. Mass Spectrom.* **2009**, *20*, 852-866.
- Frisch, M. J.; Trucks, G. W.; Schlegel, H. B.; Scuseria, G. E.; Robb, M. A.; Cheeseman, J. R.; Scalmani, G.; Barone, V.; Mennucci, B.; Petersson, G. A.; Nakatsuji, H.; Caricato, M.; Li, X.; Hratchian, H. P.; Izmaylov, A. F.; Bloino, J.; Zheng, G.; Sonnenberg, J. L.; Hada, M.; Ehara, M.; Toyota, K.; Fukuda, R.; Hasegawa, J.; Ishida, M.; Nakajima, T.; Honda, Y.; Kitao, O.; Nakai, H.; Vreven, T.; Montgomery Jr., J. A.; Peralta, J. E.; Ogliaro, F.; Bearpark, M. J.; Heyd, J.; Brothers, E. N.; Kudin, K. N.; Staroverov, V. N.; Kobayashi, R.; Normand, J.; Raghavachari, K.; Rendell, A. P.; Burant, J. C.; Iyengar, S. S.; Tomasi, J.; Cossi, M.; Rega, N.; Millam, N. J.; Klene, M.; Knox, J. E.; Cross, J. B.; Bakken, V.; Adamo, C.; Jaramillo, J.; Gomperts, R.; Stratmann, R. E.; Yazyev, O.; Austin, A. J.; Cammi, R.; Pomelli, C.; Ochterski, J. W.; Martin, R. L.; Morokuma, K.; Zakrzewski, V. G.; Voth, G. A.; Salvador, P.; Dannenberg, J. J.; Dapprich, S.; Daniels, A. D.; Farkas, Ö.; Foresman, J. B.; Ortiz, J. V.; Cioslowski, J.; Fox, D. J. *Gaussian 09, Revision D.01* Gaussian, Inc.: Wallingford, CT, USA, 2009.

- 24. Montgomery, J. A., Jr.; Frisch, M. J.; Ochterski, J. W.; Petersson, G. A., A complete basis set model chemistry. VI. Use of density functional geometries and frequencies. *J. Chem. Phys.* **1999**, *110*, 2822.
- 25. Yalcin, T.; Khouw, C.; Csizmadia, I. G.; Peterson, M. R.; Harrison, A. G., Why Are b Ions Stable Species in Peptide Spectra? *J. Am. Soc. Mass Spectrom.* **1995**, *6*, 1165-1174.
- 26. Paizs, B.; Suhai, S., Combined Quantum Chemical and RRKM Modeling of the Main Fragmentation Pathways of Protonated GGG. II. Formation of b<sub>2</sub>, y<sub>1</sub>, and y<sub>2</sub> Ions. *Rapid Commun. Mass Spectrom.* **2002**, *16*, 375-389.
- 27. El Aribi, H.; Rodriquez, C. F.; Almeida, D. R. P.; Ling, Y.; Mak, W. W.-N.; Hopkinson, A. C.; Siu, K. W. M., Elucidation of Fragmentation Mechanisms of Protonated Peptide Ions and Their Products: A Case Study on Glycylglycylglycine Using Density Functional Theory and Threshold Collision-Induced Dissociation. *J. Am. Chem. Soc.* **2003**, *125*, 9229-9236.
- 28. Yoon, S. H.; Chamot-Rooke, J.; Perkins, B. R.; Hilderbrand, A. E.; Poutsma, J. C.; Wysocki, V. H., IRMPD Spectroscopy Shows That AGG Forms an Oxazolone b<sub>2</sub><sup>+</sup> Ion. *J. Am. Chem. Soc.* **2008**, *130*, 17644-17645.
- 29. Oomens, J.; Young, S.; Molesworth, S.; van Stipdonk, M. J., Spectroscopic evidence for an oxazolone structure of the b<sub>2</sub> fragment ion from protonated tri-alanine. *J. Am. Soc. Mass Spectrom.* **2009**, *20*, 334-339.
- 30. Chen, X.; Yu, L.; Steill, J. D.; Oomens, J.; Polfer, N. C., Effect of peptide fragment size on the propensity of cyclization in collision-induced dissociation: Oligoglycine b<sub>2</sub>-b<sub>8</sub>. *J. Am. Chem. Soc.* **2009**, *131*, 18272–18282.
- 31. Wang, D.; Gulyuz, K.; Stedwell, C. N.; Polfer, N. C., Diagnostic NH and OH Vibrations for Oxazolone and Diketopiperazine Structures: b<sub>2</sub> from Protonated Triglycine. *J. Am. Soc. Mass Spectrom.* **2011**, *22*, 1197-1203.
- 32. Armentrout, P. B.; Clark, A. A., The Simplest b<sub>2</sub><sup>+</sup> Ion: Determining Its Structure from Its Energetics by a Direct Comparison of the Threshold Collision-induced Dissociation of Protonated Oxazolone and Diketopiperazine. *Int. J. Mass Spectrom.* **2012**, *316-318*, 182–191.
- 33. Polfer, N. C.; Oomens, J.; Suhai, S.; Paizs, B., Infrared Spectroscopy and Theoretical Studies on Gas-Phase Protonated Leu-enkephalin and Its Fragments: Direct Experimental Evidence for the Mobile Proton. *J. Am. Chem. Soc.* **2007**, *129*, 5887-5897.
- 34. Bythell, B. J.; Erlekam, U.; Paizs, B.; Maître, P., Infrared Spectroscopy of Fragments from Doubly Protonated Tryptic Peptides. *ChemPhysChem* **2009**, *10*, 883-885.
- 35. Armentrout, P. B.; Heaton, A. L.; Ye, S. J., Thermodynamics and Mechanisms for Decomposition of Protonated Glycine and Its Protonated Dimer. *J. Phys. Chem. A* **2011**, *115*, 11144-11155.
- 36. Armentrout, P. B.; Heaton, A. L., Thermodynamics and Mechanisms of Protonated Diglycine Decomposition: A Computational Study. *J. Am. Soc. Mass Spectrom.* **2012**, *23*, 621-631.
- 37. Armentrout, P. B.; Heaton, A. L., Thermodynamics and Mechanisms of Protonated Diglycine Decomposition: A Guided Ion Beam Study. *J. Am. Soc. Mass Spectrom.* **2012**, *23*, 632-643.
- 38. Bythell, B. J.; Barofsky, D. F.; Pingitore, F.; Polce, M. J.; Wang, P.; Wesdemiotis, C.; Paizs, B., Backbone cleavages and sequential loss of carbon monoxide and ammonia from protonated AGG: A combined tandem mass spectrometry, isotope labeling, and theoretical study. *J. Am. Soc. Mass Spectrom.* **2007**, *18*, 1291-1303.
- 39. Wu, R.; McMahon, T. B., Infrared Multiple Photon Dissociation Spectroscopy as Structural Confirmation for GlyGlyGlyH<sup>+</sup> and AlaAlaAlaH<sup>+</sup> in the Gas Phase. Evidence for Amide Oxygen as the Protonation Site. *J. Am. Chem. Soc.* **2007**, *129*, 11312-11313.
- 40. Voss, J. M.; Fischer, K. C.; Garand, E., Revealing the Structure of Isolated Peptides: IR-IR Predissociation Spectroscopy of Protonated Triglycine Isomers. *J. Mol. Spectrosc.* **2018**, *347*, 28-34.
- 41. Jones, R. M.; Boles, G. C.; Armentrout, P. B., Cis-trans isomerization is not rate determining for b<sub>2</sub> ion structures: A guided ion beam and computational study of the decomposition of H<sup>+</sup>(GlyProAla). *Int. J. Mass Spectrom.* **2020**, *458*, 116434.

- 42. Zou, S.; Oomens, J.; Polfer, N. C., Competition between diketopiperazine and oxazolone formation in water loss products from protonated ArgGly and GlyArg. *Int. J. Mass Spectrom.* **2012**, *316-318*, 12-17.
- 43. Nelson, C. R.; Abutokaikah, M. T.; Harrison, A. G.; Bythell, B. J., Proton Mobility in b<sub>2</sub> Ion Formation and Fragmentation Reactions of Histidine-Containing Peptides. *J. Am. Soc. Mass Spectrom.* **2016**, *27*, 487-497.
- 44. Rodriquez, C. F.; Cunje, A.; Shoeib, T.; Chu, I. K.; Hopkinson, A. C.; Siu, K. W. M., Proton Migration and Tautomerism in Protonated Triglycine. *J. Am. Chem. Soc.* **2001**, *123*, 3006-3012.
- 45. Allen, J. M.; Racine, A. H.; Berman, A. M.; Johnson, J. S.; Bythell, B. J.; Paizs, B.; Glish, G. L., Why Are a<sub>3</sub> Ions Rarely Observed? *J. Am. Soc. Mass Spectrom.* **2008**, *19*, 1764-1770.
- 46. Harrison, A. G., The Gas-Phase Basicities and Proton Affinities of Amino Acids and Peptides. *Mass Spectrom. Rev.* **1997**, *16*, 201-221.
- 47. Hunter, E. P. L.; Lias, S. G., Evaluated Gas Phase Basicities and Proton Affinities of Molecules: An Update. *J. Phys. Chem. Ref. Data* **1998**, *27*, 413-656.
- 48. Bouchoux, G.; Salpin, J.-Y., Gas-Phase Basicity of Glycine, Alanine, Proline, Serine, Lysine, Histidine and Some of Their Peptides by the Thermokinetic Method. *Eur. J. Mass Spectrom.* **2003**, *9*, 391-402.
- 49. Hahn, I.-S.; Wesdemiotis, C., Protonation thermochemistry of β-alanine: An evaluation of proton affinities and entropies determined by the extended kinetic method. *Int. J. Mass Spectrom.* **2003**, *222*, 465-479.
- 50. Bleiholder, C.; Suhai, S.; Paizs, B., Revising the Proton Affinity Scale of the Naturally Occurring α-Amino Acids. *J. Am. Soc. Mass Spectrom.* **2006,** *17*, 1275-1281.
- 51. Boles, G. C.; Wu, R. R.; Rodgers, M. T.; Armentrout, P. B., Thermodynamics and Mechanisms of Protonated Asparaginyl-Glycine Decomposition. *J. Phys. Chem. B* **2016**, *120*, 6525–6545.
- 52. Boles, G. C.; Wu, R. R.; Rodgers, M. T.; Armentrout, P. B., Protonated Asparaginyl-Alanine Decomposition: a TCID, SORI-CID, and Computational Analysis. *J. Am. Soc. Mass Spectrom.* **2018**, *29*, 2341-2359.
- 53. Kempkes, L. J. M.; Boles, G. C.; Martens, J.; Berden, G.; Armentrout, P. B.; Oomens, J., Deamidation of Protonated Asparagine–Valine Investigated by a Combined Spectroscopic, Guided Ion Beam, and Theoretical Study. *J. Phys. Chem. A* **2018**, *122*, 2424-2436.
- 54. Boles, G. C.; Kempkes, L. J. M.; Martens, J.; Berden, G.; Oomens, J.; Armentrout, P. B., Influence of a Hydroxyl Group on the Deamidation and Dehydration Reactions of Protonated Asparagine-Serine Investigated by Combined Spectroscopic, Guided Ion Beam, and Theoretical Approaches. J. Am. Soc. Mass Spectrom. 2021, 32, 786-805.
- 55. Boles, G. C.; Kempkes, L. J. M.; Martens, J.; Berden, G.; Oomens, J.; Armentrout, P. B., Ion Spectroscopy and Guided Ion Beam Studies of Protonated Asparaginyl-Threonine Decomposition: Influence of a Hydroxyl Containing C-Terminal Residue on Deamidation Processes. *Int. J. Mass Spectrom.* **2019**, *442*, 64-82.

Table 1: Fitting parameters of Equations S1, S3a, and S3b, threshold energies at 0 K, and entropies of activation at 1000 K for the decomposition of  $H^+GGA^a$ 

Reaction - products	TS <sup>b</sup>	$\sigma_0$	n	$E_0(eV)$	$\Delta { m S}_{1000}{}^{\dagger}$
					(J/K mol) <sup>c</sup>
$[b_2]^+(H^+AMOx) + A$	PSL	$18.6 \pm 1.0$	$0.8\pm0.1$	$1.91 \pm 0.05$	$88 \pm 5$
		$12.7 \pm 1.1$	$1.2 \pm 0.1$	$1.66 \pm 0.05$	$89 \pm 5$
2a $[y_1 + 2H]^+ (H^+A) + AMOx$	PSL	$18.6 \pm 1.0$	$0.8\pm0.1$	$1.88 \pm 0.06^{\circ}$	$63 \pm 6$
		$12.7 \pm 1.1$	$1.2 \pm 0.1$	$1.63 \pm 0.05^{\circ}$	$64 \pm 6$
4 $[y_2 + 2H]^+ (H^+GA) + CO + CH_2NH$	PSL	$18.6 \pm 1.0$	$0.8\pm0.1$	$\leq 2.31\pm0.05^{\rm d}$	$135\pm5$
		$12.7 \pm 1.1$	$1.2 \pm 0.1$	$\leq 1.98 \pm 0.05^{d}$	$125\pm6$
5a $[a_1]^+$ (CH <sub>2</sub> NH <sub>2</sub> <sup>+</sup> ) CO + GA	PSL	$18.6 \pm 1.0$	$0.8\pm0.1$	$2.67\pm0.05$	$181 \pm 5$
		$12.7 \pm 1.1$	$1.2 \pm 0.1$	$2.35 \pm 0.05$	$182 \pm 5$
$3 [b_3]^+ (H^+GAMMOx) + H_2O$	$TS[O^{1t}-O^4]$	$12.7 \pm 1.1$	$1.2 \pm 0.2$	$1.29\pm0.04^{\rm e}$	$55 \pm 2$
6 $[a_2]^+([b_2]^+-CO)$	$[b_2]^+$ (PSL) $\rightarrow$ TS(H <sup>+</sup> AMOx)	$72.7 \pm 13.2$	$1.2 \pm 0.1$	$3.24\pm0.09$	42 ± 1
$2b [y_1 + 2H]^+_{HE} (H^+A)$	$[y_2 + 2H]^+(PSL) \to TS[N^3]-tt$	$62.8 \pm 11.8$	$1.2\pm0.1$	$\leq 4.19 \pm 0.12$	46 ± 1
	$[y_2 + 2H]^+(PSL) \to PSL$	$80.6 \pm 14.9$	$1.2\pm0.1$	$\leq 4.91 \pm 0.08$	$163 \pm 5$
7 m/z 44 (CH <sub>3</sub> CHNH <sub>2</sub> <sup>+</sup> )	$[y_1 + 2H]^+ \to TS[N^3 - O^4] - c$	$35.1 \pm 1.1$	$1.2 \pm 0.1$	$2.78 \pm 0.05$	61 ± 1
$8 [a_3]^+ ([b_3]^+ - CO)$	$[b_3]^+ \rightarrow TS(H^+GAMMOx)$	$21.6 \pm 4.7$	$1.2 \pm 0.1$	$2.19 \pm 0.04$	34 ± 1

 $<sup>^{</sup>a}$  In all cases, competition among  $[b_{2}]^{+}$ ,  $[y_{1}+2H]^{+}$ ,  $[y_{2}+2H]^{+}$ ,  $[a_{1}]^{+}$ , and  $[b_{3}]^{+}$  were included in the modeling. Values in bold indicate

analysis of zero-pressure extrapolated data and normal font indicate analysis of medium-pressure data using the TpLpLp model.  $^b$  PSL = phase space limit. TS[O<sup>1t</sup>-O<sup>4</sup>] = TS([O<sup>1t</sup>-O<sup>4</sup>]-ctgtt{C~O<sup>4</sup>H}), TS(H<sup>+</sup>AMOx) = TS(H<sup>+</sup>AMOx[N<sup>2</sup>]-c{OC~O})  $^{32}$ , TS[N<sup>3</sup>]-tt = TS([N<sup>3</sup>]-tt{N<sup>2</sup>C~CO<sup>2</sup>~N<sup>3</sup>C}), TS[N<sup>3</sup>-O<sup>4</sup>]-c = TS([N<sup>3</sup>-O<sup>4</sup>]-c{CC~O<sup>4</sup>H}), and TS(H<sup>+</sup>GAMMOx) = TS(H<sup>+</sup>GAMMOx[N<sup>3</sup>]-ctg(cg){C~CO<sup>3</sup>}). An arrow indicates a sequential process with the indicated TSs for the initial and sequential steps.  $^c$  Value when PSL TS frequencies below 900 cm<sup>-1</sup> of the [y<sub>1</sub> + 2H]<sup>+</sup> product in T<sub>P</sub>L<sub>P</sub>L<sub>P</sub> model are scaled by 1.1 in both medium-pressure and zero-pressure extrapolated data.  $^d$  Value when PSL TS frequencies below 900 cm<sup>-1</sup> of the [y<sub>2</sub> + 2H]<sup>+</sup> product in T<sub>P</sub>L<sub>P</sub>L<sub>P</sub> model are scaled by 1.29 in the medium-pressure data and 1.22 zero-pressure extrapolated data.  $^c$  Value when TTS frequencies below 900 cm<sup>-1</sup> of the [b<sub>3</sub>]<sup>+</sup> product are scaled by 0.77 in medium pressure data.

Table 2: Comparison of experimental and theoretical reaction energies (kJ/mol) at 0 K for decomposition of H+GGA

Products	Transition state <sup>a</sup>	Experiment <sup>b</sup>		Theory <sup>c</sup>			
		this work	literature <sup>d</sup>	B3LYP	B3LYP-D3	MP2	M06-2X
$[b_2]^+ (H^+AMOx) + G$	PSL	$186 \pm 5$		157	178	176	177
$[y_1 + 2H]^+ (H^+A) + AMOx$	PSL	$182\pm6$		169	190	182	186
$[b_3]^+ (H^+GAMMOx) + H_2O$	$TS[O^{1t}-O^4]$	$153\pm6$		123	112	103	128
$[y_2 + 2H]^+ (H^+GA) + CO + CH_2NH$	PSL	$\leq$ 224 $\pm$ 5		173	205	185	200
$[a_1]^+ (CH_2NH_2^+) + CO + AG$	PSL	$\leq$ 258 $\pm$ 5		245	262	245	263
$[a_2]^+ + CO + G$	$[b_2]^+ \rightarrow TS(H^+AMOx)$	$341\pm10$	$327 \pm 6^{\text{d}}$	289	311	302	315
			$322\pm13^{e}$				
$[y_1 + 2H]^+_{HE} + 2CH_2NH + 2CO$	$[y_2 + 2H]^+ \to PSL$	$\leq 503 \pm 9$		340	393	369	398
	$[y_2 + 2H]^+ \rightarrow TS [N^3]$ -tt	$\leq$ 433 $\pm$ 12					
m/z 44 CH <sub>3</sub> CH=NH <sub>2</sub> <sup>+</sup>	$[y_1 + 2H]^+ \to TS[N^3-O^4]$	$296\pm7$		310	333	317	336
$[a_3]^+ + CO + H_2O$	$[b_3]^+ \rightarrow TS(H^+GAMMOx)$	$240\pm 6$		222	229	218	243
$\mathrm{MAD^f}$				$27\pm16$	$16 \pm 15$	$22 \pm 21$	$13 \pm 10$
MAD <sup>g</sup>	odi magralt odi	0411)	T+ 1 1 (O )	$27 \pm 16$	20 ± 15	$24 \pm 17$	17 ± 14

a PSL = phase space limit. TS[O¹¹-O⁴] = TS([O¹¹-O⁴]-ctgtt{C~O⁴H}), TS(H⁺AMOx) = TS(H⁺AMOx[N²]-c{OC~O})  $^{32}$ , TS[N³]-tt = TS([N³]-tt{N²C~CO²~N³C}), TS[N³-O⁴] = TS([N³-O⁴]-c{CC~O⁴H}), and TS(H⁺GAMMOx) = TS(H⁺GAMMOx[N³]-ctg(cg){C~CO³}). b Experimental values from Table 1 where medium-pressure threshold energies are corrected to approximate single pressure conditions by adding  $0.29 \pm 0.04$  eV and includes deviations from using reactant [N¹]-ttggtgtt (see text). Values are given for the T<sub>P</sub>L<sub>P</sub>L<sub>P</sub> model. c Computational results from Tables S2 and S3. d Ref. 3². e Ref. 10. f Mean absolute deviation (MAD) from experimental energies of all five primary products, g MADs from experimental energies for all products except [y₁ + 2H]+HE.

Figure Captions

**Scheme 1.** Schematic reaction mechanism for H<sup>+</sup>GGA decomposition.

**Figure 1**. Cross sections for collision-induced dissociation of  $H^+GGA$  (m/z 204) with xenon at 0.1 mTorr as a function of kinetic energy in the center-of-mass (CM) frame (lower x-axis) and laboratory frame (Lab) (upper x-axis). Products are identified by their mass-to-charge ratio and the all explicit nomenclature for fragment ions. Open symbols show the primary products and closed symbols show the products formed by sequential dissociation using the same symbol and color. The solid line shows the total cross section.

**Figure 2**. H<sup>+</sup>GGA conformers, [O<sup>1t</sup>]-ctgttttt, [O<sup>1t</sup>]-ctgttgtt, [N<sup>1</sup>]-ttggtgtt, (with trans peptide bonds), [N<sup>1</sup>]-tcgctgtt, [N<sup>1</sup>]-gcgttgtt, and [N<sup>1</sup>]-gcgtttttt (with one cis peptide bond) with their relative energies in kJ/mol at B3LYP, B3LYP-D3, MP2, and M06-2X levels of theory. Dashed lines denote the hydrogen bonds within the conformers.

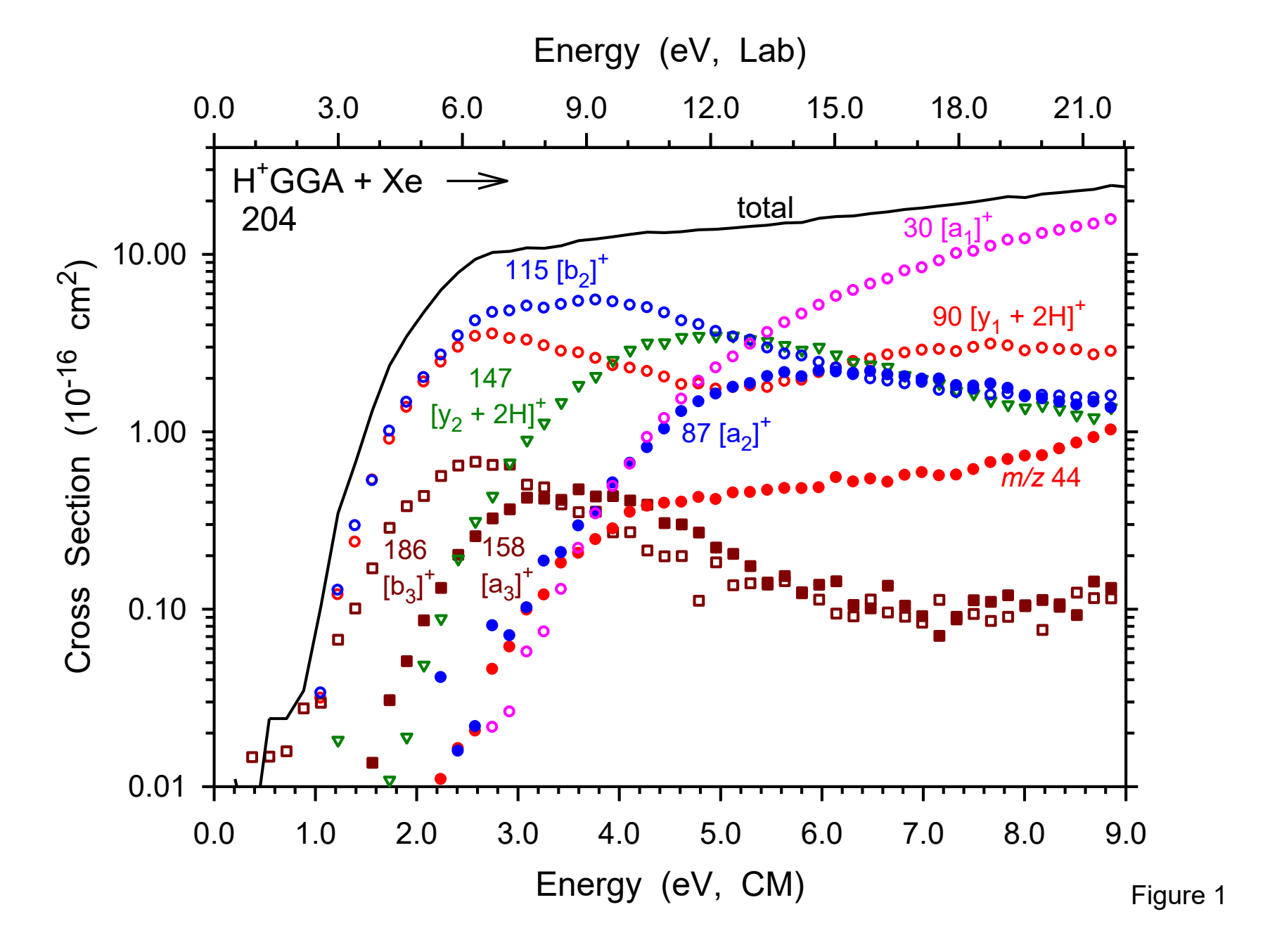
**Figure 3**. Key transition states and product ions of H<sup>+</sup>GGA decomposition with their relative energies including the energies of the neutrals lost, in kJ/mol at B3LYP, B3LYP-D3, MP2, and M06-2X levels of theory. Dashed lines denote breaking and making of bonds.

**Figure 4**. Competitive modeling of the five primary products: composite cross sections of  $[b_2]^+_{tot}$ ,  $[y_1 + 2H]^+_{tot}$ ,  $[y_2 + 2H]^+_{tot}$ ,  $[a_1]^+$ , and  $[b_3]^+_{tot}$  from CID of H<sup>+</sup>GGA with Xe using the T<sub>P</sub>L<sub>P</sub>L<sub>P</sub> model. Symbols show medium-pressure (0.1 mTorr) data for the indicated products as a function of collision energy in the center-of-mass frame (lower x-axis) and laboratory frame (upper x-axis). Solid lines show the best fit to the data using the model in Supporting Equation S1 convoluted over the neutral and ion kinetic energy distributions. Dashed lines show the model cross sections in the absence of experimental kinetic energy broadening for reactants with internal energies at 0 K.

**Figure 5**. Sequential modeling of the (a)  $[a_2]^+$  formed from  $[b_2]^+$ , (b)  $[y_1 + 2H]^+$  He ion formed from  $[y_2 + 2H]^+$  via PSL, (c) m/z 44 from  $[y_1 + 2H]^+$ , and (d)  $[a_3]^+$  ion formed from  $[b_3]^+$  along with competitive modeling of the remaining primary ions. Symbols show medium-pressure (0.1 mTorr) data for the indicated processes between H<sup>+</sup>GGA and Xe as a function of collision energy in the center-of-mass frame (lower x-axis) and in the laboratory frame (upper x-axis). The product cross sections,  $[a_1]^+$  in (a) and (b),  $[b_3]^+$  in (c), and  $[y_2 + 2H]^+$  in (d) are not shown for purposes of clarity. Solid lines show the best fit to the data using the models in Equations S1, S3a, and S3b convoluted over the neutral and ion kinetic energy distributions. Dashed lines show the model cross sections in the absence of experimental kinetic energy broadening for reactants with internal energies at 0 K.

**Figure 6**. Comparison of experimental threshold energies for the products shown modeled using Equations S1 and S3 with B3LYP (red triangles), B3LYP-D3 (blue circles), MP2 (purple squares), and M06-2X (green triangles) energies taken from Table 2. The diagonal line indicates perfect agreement between theory and experiment.

Figure 7. Cross sections for major primary and secondary products formed in the CID of H<sup>+</sup>GGA (symbols), H<sup>+</sup>GGG (solid lines) and H<sup>+</sup>GAG (dashed lines) with xenon as a function of kinetic energy in the center-of-mass frame (CM, lower x-axis).



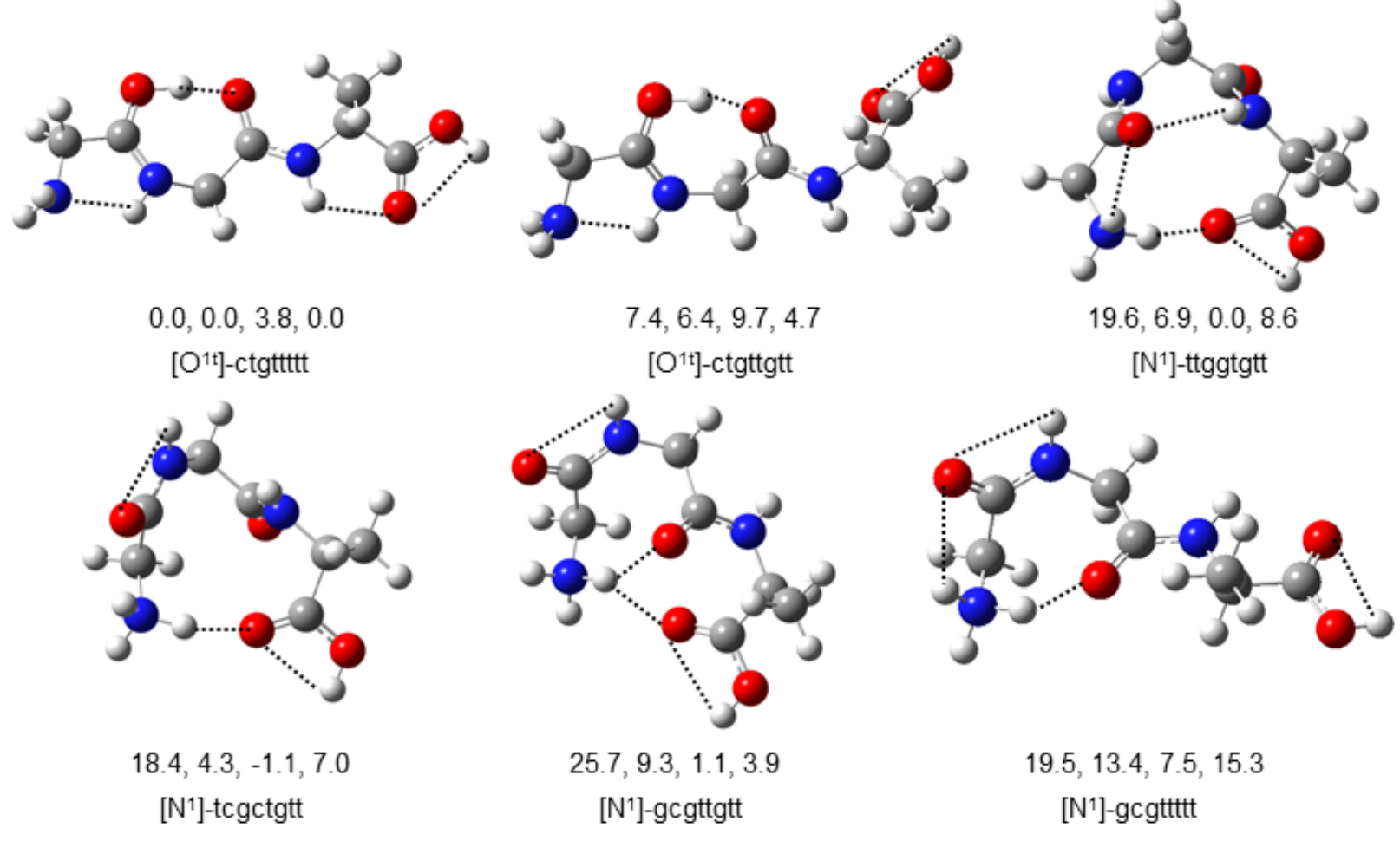


Figure 2

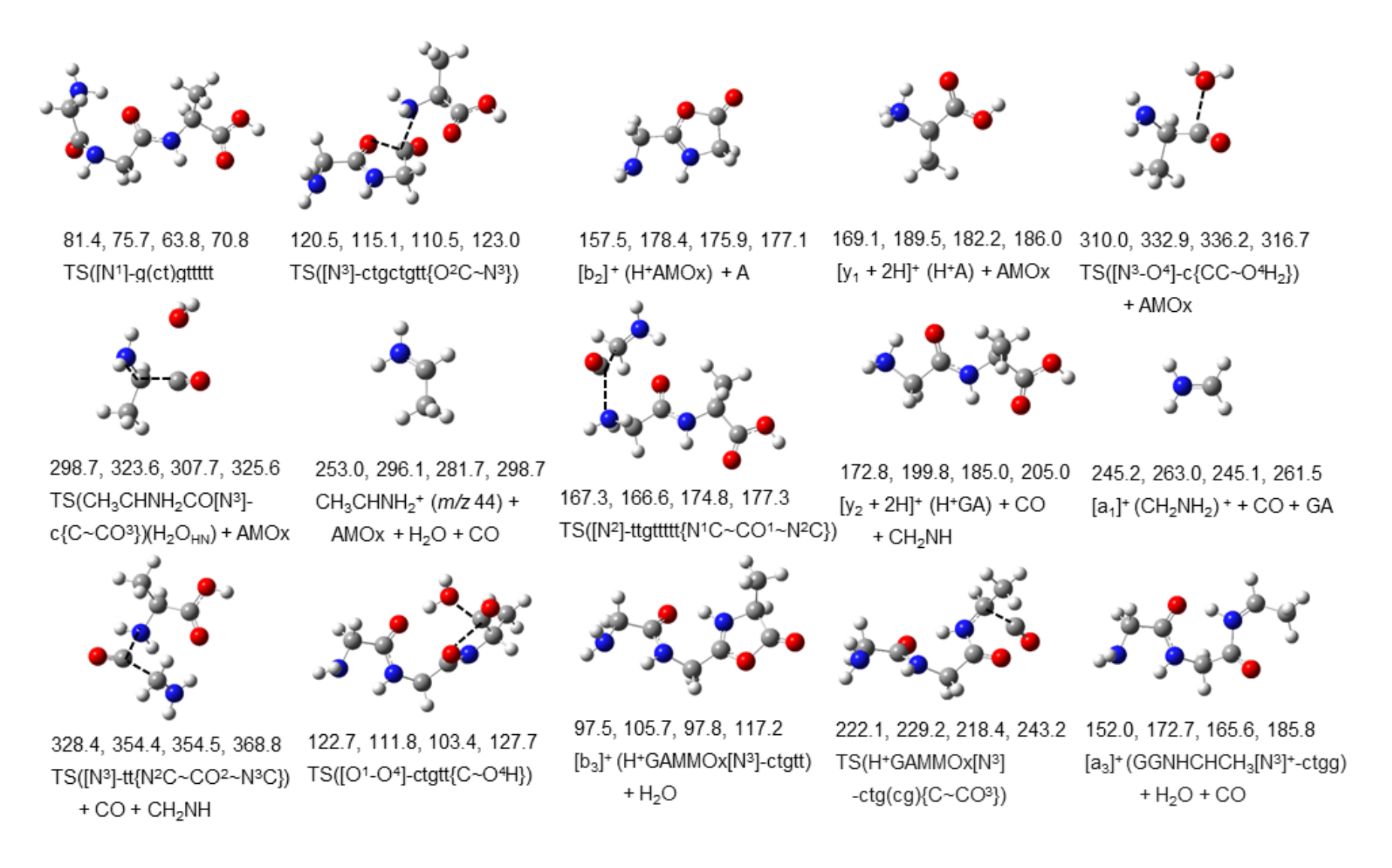


Figure 3

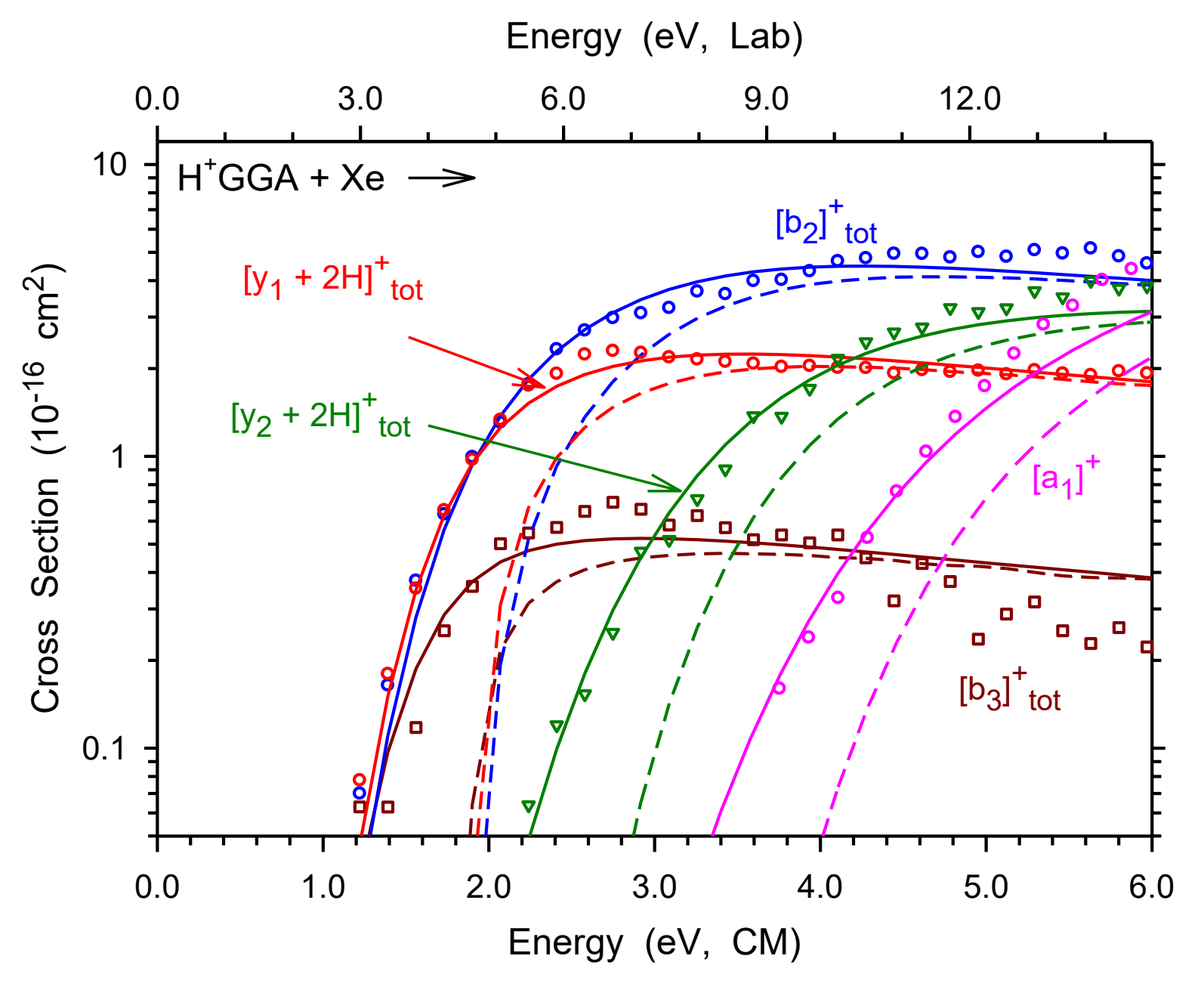


Figure 4

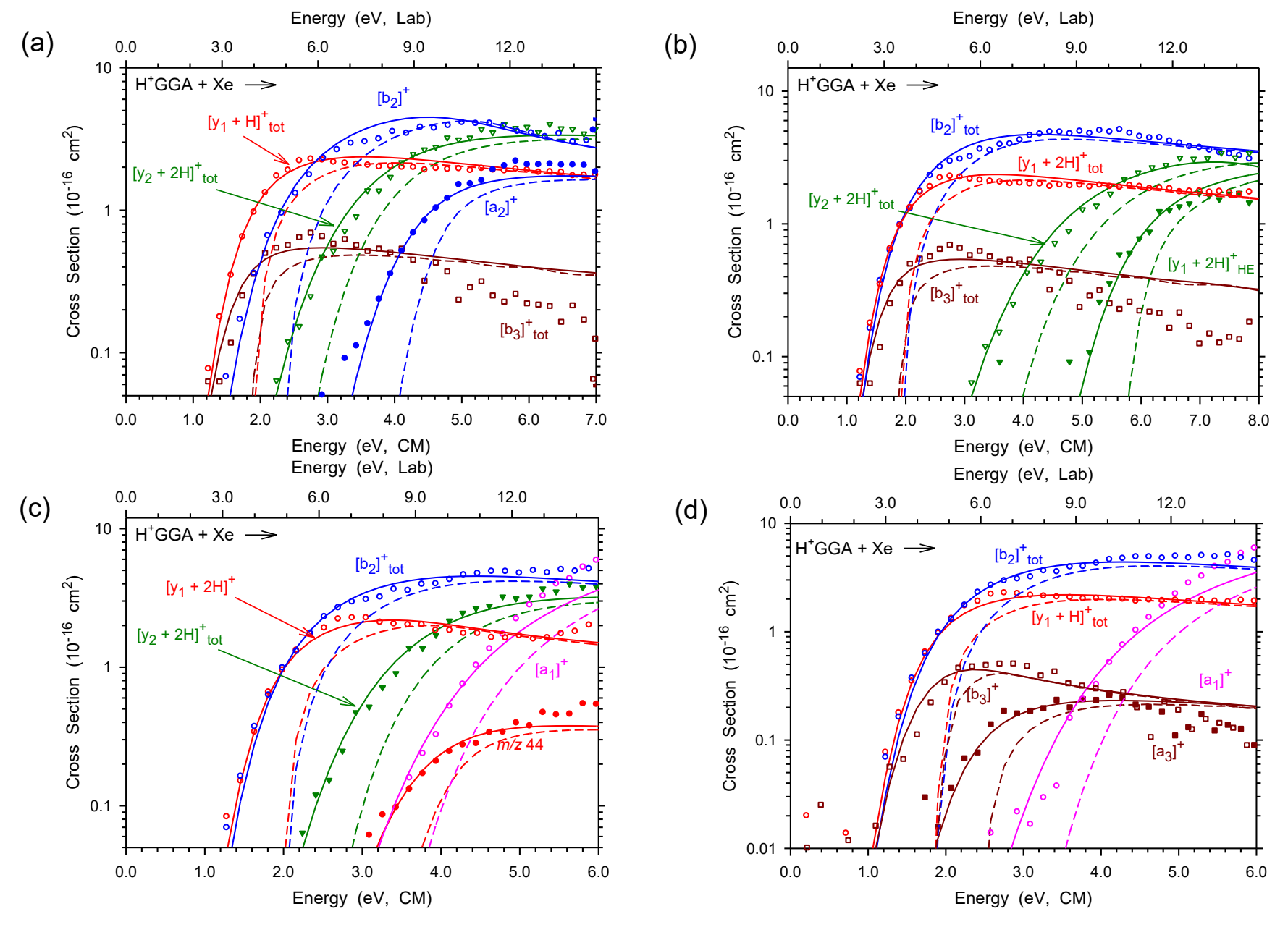


Figure 5

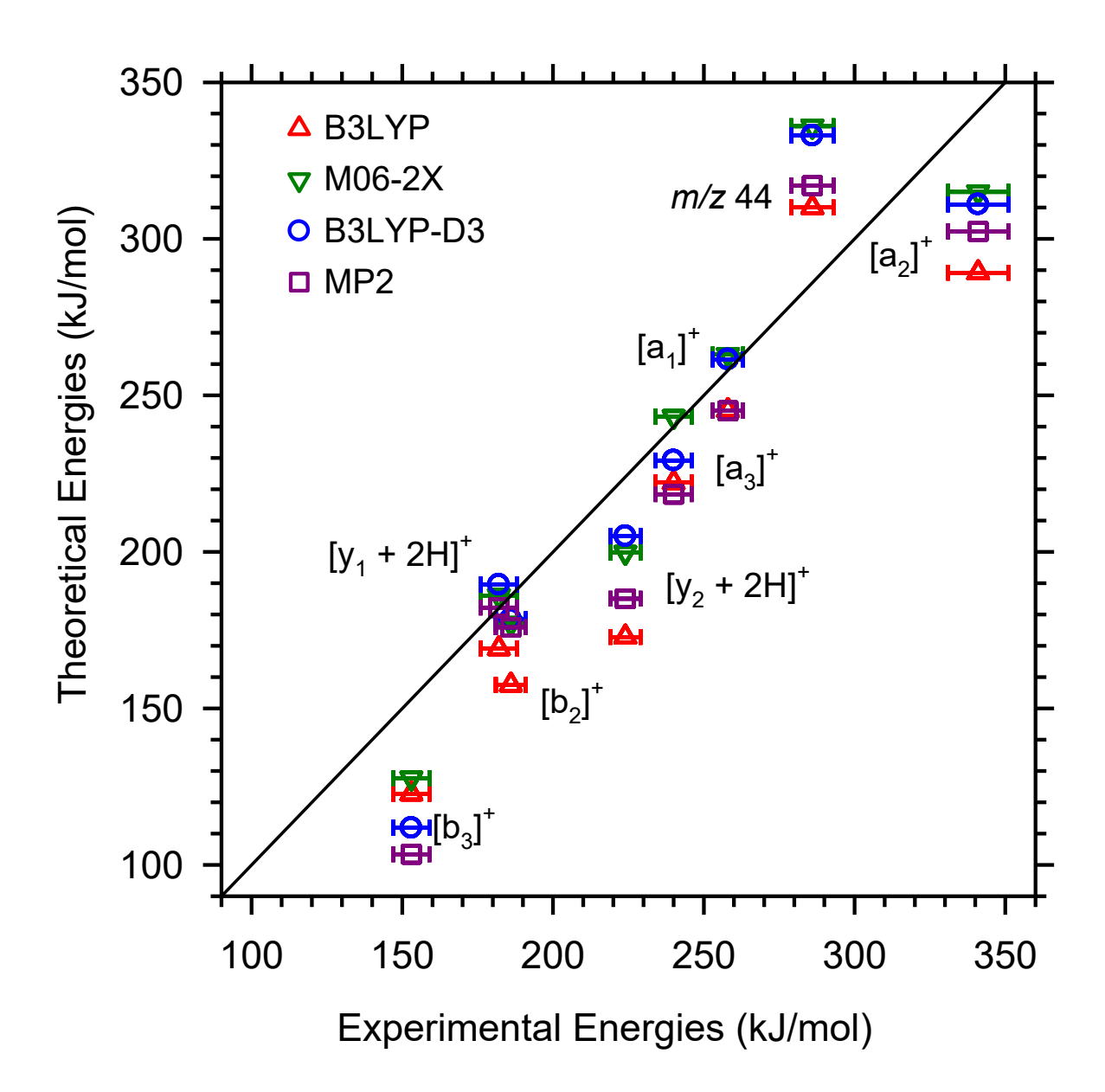


Figure 6

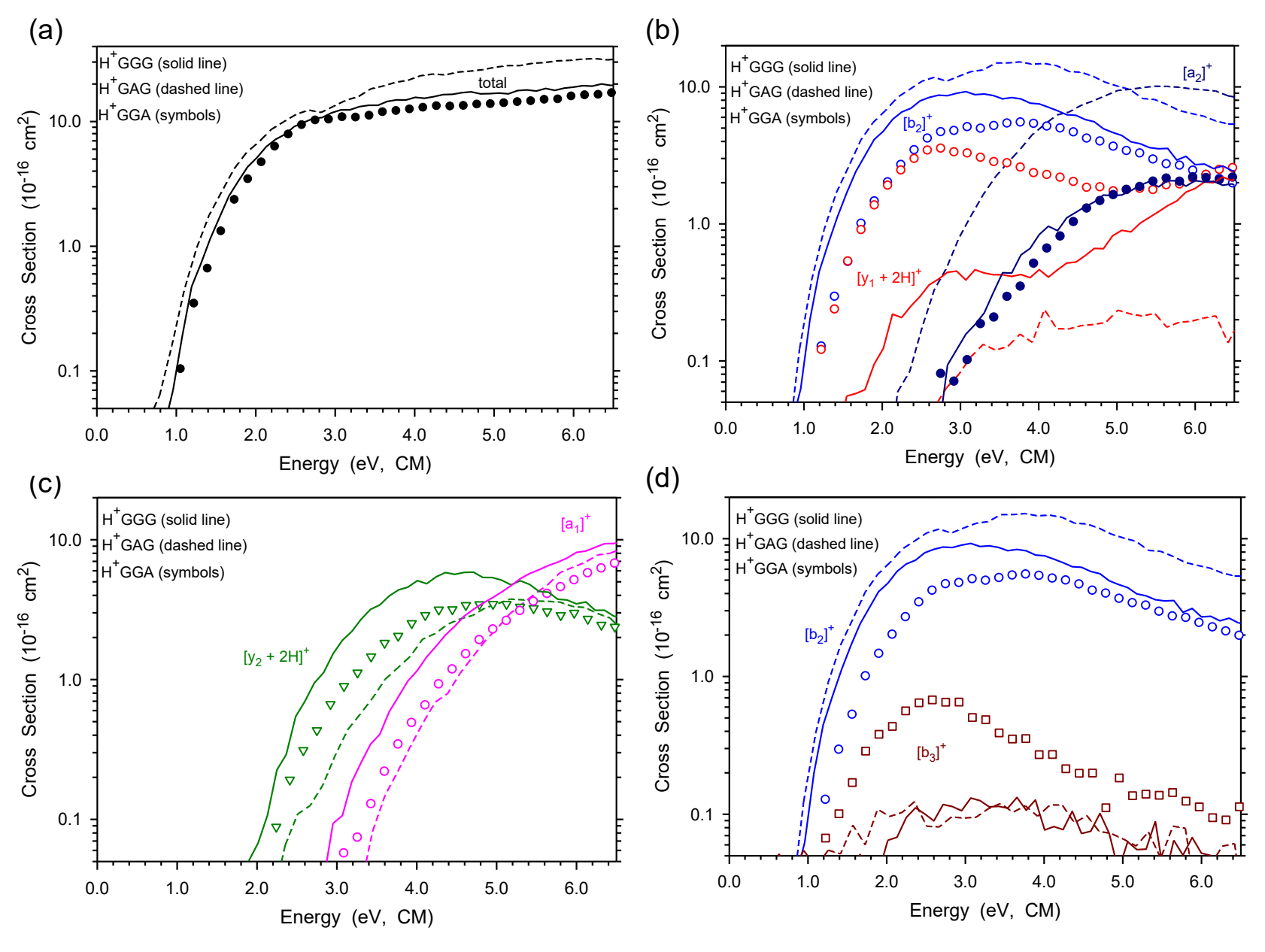
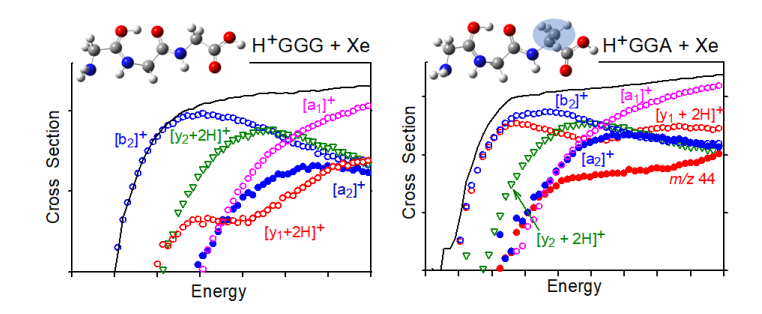


Figure 7

## For Table of Contents Use Only

Thermodynamics and Reaction Mechanisms for Decomposition of a Simple Protonated Tripeptide, H<sup>+</sup>GGA: From H<sup>+</sup>GGG to H<sup>+</sup>GAG to H<sup>+</sup>GGA

## A. Mookherjee and P. B. Armentrout\*



Kinetic energy dependent cross sections for fragmentation of protonated glycylglycylalanine (GGA) show distinct differences compared with previous work on glycylglycylglycine (GGG) and glycylalanylglycine (GAG).